

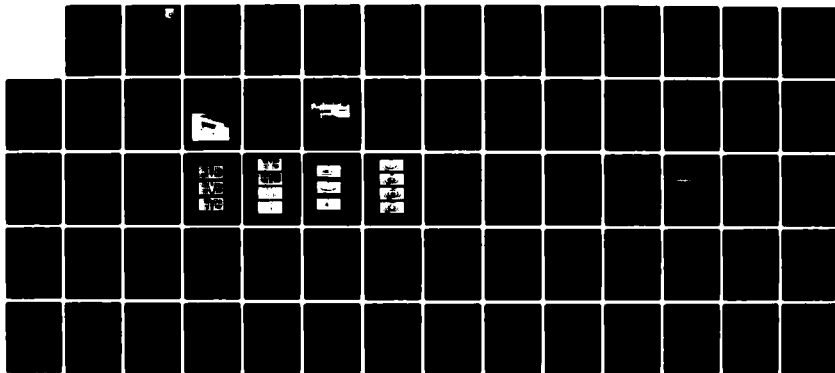
AD-A129 416

STRAINS FROM PROJECTION MOIRE DATA(U) DAYTON UNIV OH
RESEARCH INST B B RAJU ET AL. FEB 83 UDR-TR-82-142
AFWAL-TR-83-3020 F33615-80-C-3401

1/1

UNCLASSIFIED

F/G 20/11 NL



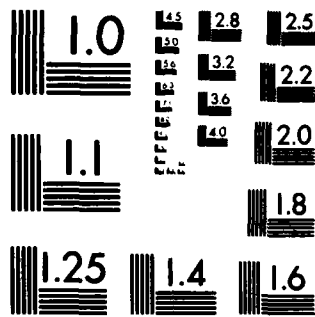
END

DATE

FILMED

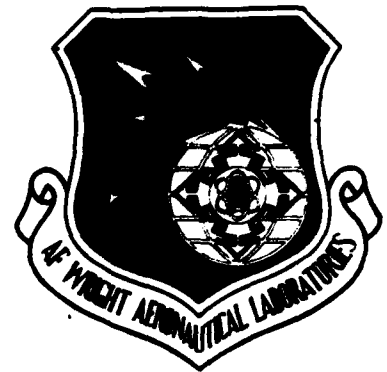
7 83

DTIC



MICROCOPY RESOLUTION TEST CHART
NATIONAL BUREAU OF STANDARDS-1963-A

2
AFWAL-TR-83-3020



STRAINS FROM PROJECTION MOIRÉ DATA

B. Basava Raju
Blaine S. West
Andrew J. Piekutowski

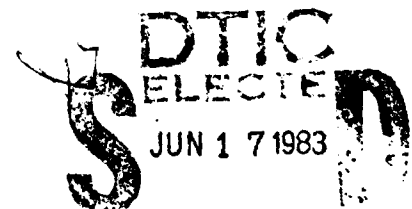
University of Dayton Research Institute
Dayton, Ohio 45469

Final Report for Period September 1981 - March 1982.

February 1983

Approved for public release; distribution unlimited.

FLIGHT DYNAMICS LABORATORY
AIR FORCE WRIGHT AERONAUTICAL LABORATORIES
AIR FORCE SYSTEMS COMMAND
WRIGHT-PATTERSON AIR FORCE BASE, OHIO 45433



A

83 06 16 077

AD A129416


DTIC FILE COPY


NOTICE

When Government drawings, specifications, or other data are used for any purpose other than in connection with a definitely related Government procurement operation, the United States Government thereby incurs no responsibility nor any obligation whatsoever; and the fact that the government may have formulated, furnished, or in any way supplied the said drawings, specifications, or other data, is not to be regarded by implication or otherwise as in any manner licensing the holder or any other person or corporation, or conveying any rights or permission to manufacture, use, or sell any patented invention that may in any way be related thereto.

This report has been reviewed by the Office of Public Affairs (ASD/PA) and is releasable to the National Technical Information Service (NTIS). At NTIS, it will be available to the general public, including foreign nations.

This technical report has been reviewed and is approved for publication.


Robert J. Simmons, 1LT. USAF
Project Manager
Improved Windshield Protection ADPO
Vehicle Equipment Division


Ralph J. Speelman
Program Manager
Improved Windshield Protection ADPO
Vehicle Equipment Division

FOR THE COMMANDER


Solomon R. Metres
Director
Vehicle Equipment Division

"If your address has changed, if you wish to be removed from our mailing list, or if the addressee is no longer employed by your organization please notify AFWAL/FIEA, W-PAFB, OH 45433 to help us maintain a current mailing list".

Copies of this report should not be returned unless return is required by security considerations, contractual obligations, or notice on a specific document.

UNCLASSIFIED

SECURITY CLASSIFICATION OF THIS PAGE (When Data Entered)

REPORT DOCUMENTATION PAGE		READ INSTRUCTIONS BEFORE COMPLETING FORM
1. REPORT NUMBER AFWAL-TR-83-3020	2. GOVT ACCESSION NO. AD-A129 400	3. RECIPIENT'S CATALOG NUMBER
4. TITLE (and Subtitle) STRAINS FROM PROJECTION MOIRÉ DATA		5. TYPE OF REPORT & PERIOD COVERED Final Report for Period Sept. 1981 - March 1982
		6. PERFORMING ORG. REPORT NUMBER UDR-TR-82-142
7. AUTHOR(s) B. Basava Raju Blaine S. West Andrew J. Piekutowski		8. CONTRACT OR GRANT NUMBER(s) F33615-80-C-3401
9. PERFORMING ORGANIZATION NAME AND ADDRESS University of Dayton Research Institute 300 College Park Avenue Dayton, Ohio 45469		10. PROGRAM ELEMENT, PROJECT, TASK AREA & WORK UNIT NUMBERS PE 64212F, Task 192601, Project 1926, Work Unit 19260104
11. CONTROLLING OFFICE NAME AND ADDRESS Flight Dynamics Laboratory (AFWAL/FIER) AF Wright Aeronautical Laboratories, AFSC Wright-Patterson Air Force Base, OH 45433		12. REPORT DATE February 1983
		13. NUMBER OF PAGES 63
14. MONITORING AGENCY NAME & ADDRESS (if different from Controlling Office)		15. SECURITY CLASS. (of this report) Unclassified
		15a. DECLASSIFICATION/DOWNGRADING SCHEDULE
16. DISTRIBUTION STATEMENT (of this Report) Approved for public release; distribution unlimited.		
17. DISTRIBUTION STATEMENT (of the abstract entered in Block 20, if different from Report)		
18. SUPPLEMENTARY NOTES		
19. KEY WORDS (Continue on reverse side if necessary and identify by block number) Strains from moiré deformations, projection moiré Static response analysis Four-point bending test and analysis Large deflection beam theory, plate theory		
20. ABSTRACT (Continue on reverse side if necessary and identify by block number) The main objective of this program was to determine and evaluate the surface strains from out-of-plane deformations determined by the projection moiré method of large surfaces experiencing static loads. The program consisted of three primary tasks: (1) design of an experiment consisting of a four-point bending fixture and a 26x6x1/4 inch flat test specimen, moiré device, strain gage instrumentation, and dial gages, and the collection of experimental data for various static loads; (2) analytical prediction of the		

DD FORM 1 JAN 73 1473 EDITION OF 1 NOV 65 IS OBSOLETE

UNCLASSIFIED

SECURITY CLASSIFICATION OF THIS PAGE (When Data Entered)

UNCLASSIFIED

SECURITY CLASSIFICATION OF THIS PAGE(When Data Entered)

Continuation, block 20.

cont → deflections and strains by small and large deflection beam theories and small deflection plate theory; (3) computation of strains from the moiré deflections by a number of numerical curve fitting techniques; and (4) comparison of the strains determined from the moiré technique with experimental and theoretical strains.

Tests were conducted at loads from 50 to 300 pounds in 50 pound load increments and strains were computed from moire deflections by using second and third order polynomials and a second order Legendre polynomial. Both the deflections and strains were accurately determined for the flat surfaces investigated. It is recommended that the investigations be extended to evaluate the accuracy of the method for curved surfaces under dynamic response conditions.

UNCLASSIFIED

SECURITY CLASSIFICATION OF THIS PAGE(When Data Entered)

FOREWORD

The effort reported herein was conducted for the Air Force Wright Aeronautical Laboratories, Flight Dynamics Laboratory, Wright-Patterson Air Force Base, Ohio, under Contract F33615-80-C-3401, Project 1926. Air Force administrative direction and technical support was provided by Lt. Robert Simmons, AFWAL/FIEA. The work described herein was conducted during the period September 1981 to March 1982. Project supervision was provided by Mr. Dale H. Whitford, Supervisor, Aerospace Mechanics Division, University of Dayton Research Institute. Experimental support was provided by the Impact Physics Group of the Experimental and Applied Mechanics Division.

The authors wish to acknowledge the contributions of Mr. Keith Miller who assisted in the use of PLSCF, PLOTS programs for curve-fitting the experimental data, and Ms. Susan A. Emery and Mr. Paul E. Johnson for helping in strain gage instrumentation and load cell calibration.



Accession For	
NTIS GRA&I	<input checked="checked" type="checkbox"/>
NTIS TAB	<input type="checkbox"/>
Unannounced	<input type="checkbox"/>
Justification	
Distribution/	
Availability Codes	
Dist	Avail and/or Special
A	

TABLE OF CONTENTS

SECTION	PAGE
1 INTRODUCTION	1
1.1 Background Information	1
1.2 Program Objective and Summary	1
2 EXPERIMENTAL TECHNIQUES	3
2.1 Test Specimen	3
2.2 Four-Point Bending Load Device	3
2.3 Instrumentation	5
2.4 Matrix for Experimental Investigations	5
3 ANALYTICAL TECHNIQUES	10
3.1 Small-Deflection Plate Theory	10
3.2 Large-Deflection Beam Theory	11
4 EXPERIMENTAL AND ANALYTICAL RESULTS	16
4.1 Experimental Procedure	16
4.2 Moiré Results	17
4.3 Deflections from Dial Gages	22
4.4 Strains from Electrical Resistance Gages	34
4.5 Analytical Results	34
5 ANALYSIS OF RESULTS	39
6 CONCLUSIONS AND RECOMMENDATIONS	46
APPENDIX A: Small Deflection Plate Theory for Four-Point Bending Plate Specimens	47
APPENDIX B: Large Deflection Beam Theory for a Four-Point Bending Beam Specimen	50
REFERENCES	55

LIST OF ILLUSTRATIONS

FIGURE		PAGE
1	Four-Point Bending Specimen	4
2	Four-Point Bending Load Device	4
3	Moiré Device with Four-Point Bending Load Fixture	6
4	Schematic View of Moiré Device Illustrating Components and their Relationship to Target	7
5	Four-Point Bending Plate Specimen	8
6	Four-Point Bending Beam Specimen	12
7	Moiré Fringes to Determine $\frac{\partial^2 w}{\partial x^2}$ Curvature	18
8	Moiré Fringes to Determine $\frac{\partial^2 w}{\partial y^2}$ Curvature	20
9	Comparison of Experimental and Analytical Deflections	25
10	Comparison of Experimental and Analytical Strains	26
11	Regression Analysis Using a Second-Order Polynomial Relating Deflections and Span Positions	27
12	Regression Analysis Using a Second-Order Legendre Polynomial Relating Deflections and Span Positions	30

LIST OF TABLES

TABLE		PAGE
1	Test Matrix	9
2	Moiré Deflections and Strains at the Beam Center	23
3	Moiré Deflections and Strains Three Inches Below Center	24
4	Dial Gage Deflections at Center of Beam	33
5	Strains from Resistance Strain Gages	35
6	Deflections and Strains from Small-Deflection Beam Theory	36
7	Deflections and Strains from Small-Deflection Plate Theory	37
8	Deflections and Strains by Large-Deflection Beam Theory	38
9	Comparison of Deflections: Moiré, Dial Gage, Beam Theories, and Plate Theory	40
10	Comparisons of ϵ_x Strains: Moiré, Resistance Gages, Beam Theories, Plate Theory	41
11	Comparison of Moiré Strains (by Legendre Polynomials) with Resistance Gages	42
12	Comparison of ϵ_y Strains: Moiré, Resistance Gages, Beam Theories, Plate Theory	43

LIST OF SYMBOLS

A, B, C	= Points of the symmetry, the loading, and the tip of the four-point bending beam specimen
A_m, B_m	= Amplitudes of displacements in plate specimen, in.
a, b	= Length and width of the four-point bending plate specimen, in.
C^*, C_1, C_2	= Constants of integration in the large deflection beam theory
D	= Flexural rigidity of beam - $EI/1-\nu^2$, in ² -lbs.
\bar{D}	= Flexural rigidity of plate - $Eh^3/12(1-\nu^2)$, in-lbs.
E	= Young's modulus, psi.
$E(p, \bar{m})$	= Elliptic integral of second kind - $\int_0^{\bar{m}} (1-p^2 \sin^2 \phi)^{1/2} d\phi$
$E(p)$	= Complete elliptic integral of second kind - $\int_0^{\pi/2} (1-p^2 \sin^2 \phi)^{1/2} d\phi$
h	= Thickness of specimen, in.
I	= Moment of inertia of cross section of beam - $bh^3/12$, in ⁴ .
j	= Summation subscript, 1 and 2.
$K(p, \bar{m})$	= Elliptic integral of the first kind - $\int_0^{\bar{m}} (1-p^2 \sin^2 \phi)^{-1/2} d\phi$
$K(p)$	= Complete elliptic integral of the first kind - $\int_0^{\pi/2} (1-p^2 \sin^2 \phi)^{-1/2} d\phi$
K_1	= Load parameter used in the large deflection beam theory - $\{P(\cot \psi_0 - \cot \lambda_0)/D\}^{1/2}$, in ⁻¹

LIST OF SYMBOLS, continued

- K_2 = Load parameter used in the large deflection beam theory - $\{P/D \sin \psi_0\}^{1/2}$, in^{-1}
- L_1, L_2 = Lengths of the regions AB and BC of the four-point bending beam specimen, in.
- M_x, M_y = Bending moments per unit length of sections of a plate perpendicular to x- and y-axes, respectively in.-lbs.in^{-1} .
- M_{xy} = Twisting moments per unit length of section of a plate perpendicular to x-axis, in.-lbs.-in^{-1} .
- M_U, M_Q = Bending moments at points U and Q on the four-point bending beam, in.-lbs.
- m = Summation subscript, 1,3,5,... ∞ ...
- \bar{m} = A parameter used in the large deflection beam theory - $\text{Sin}^{-1}[\{\text{Sin}(\overline{\psi_1 + \psi_0})/2\}/p]$
- N = A parameter used in the large deflection beam theory - $\text{Sin}^{-1}[\text{Sin}(\psi_1/2)/p]$
- n = A parameter used in the large deflection beam theory - $\text{Sin}^{-1}[\{\text{Sin}(\overline{\psi + \psi_0})/2\}/p]$
- P = Concentrated point load on the beam or total line load on the plate specimen, lbs.
- p = A parameter used in the large deflection beam theory - $\text{Sin} \pi/4$
- P_1 = A parameter used in the large deflection beam theory - $2^{-1/2}\{1 - \cos \psi_1 + K_2^2/K_1^2 [\cos(\pi/2 - \psi_1 + \psi_2)]\}^{1/2}$
- Q = A point in the region AB of the four-point bending specimen
- q = Intensity of a continuously distributed load, psi.
- R_x, R_y = Radii of curvature of the plate in the xz- and yz-planes, in.

LIST OF SYMBOLS, continued

u	= A variable used in the large deflection beam theory = S/L_2
W, W_P, W_{CEN}	= Deflections at any general point, at the point of load application and at the center of the specimen, in.
W_D, W_M	= Center deflections of specimen determined by dial gage and by moiré method, respectively, in.
W_{PL}, W_{LBM}, W_{BM}	= Center deflections of specimen determined by plate theory, large deflection beam theory and classical beam theory, in.
x, y, z	= Cartesian coordinates
X_B, X_C	= Lengths of the regions AB and AC of the beam specimen, in.
Y_B, Y_C	= Vertical displacements of the loading point B and the tip of the beam specimen, in.
α_m	= Aspect ratio parameter of the plate specimen, $m\pi b/a$
ϵ_x, ϵ_y	= Strains in x- and y-directions, $\mu\text{in./in.}$
$\epsilon_{x1}, \epsilon_{y1}$	= Strains in the center and on the outer surface of the specimen - $\mu\text{in./in.}$
$\epsilon_{x2}, \epsilon_{y2}$	= Strains in the center and on the inner surface of the specimen - $\mu\text{in./in.}$
$\epsilon_{XA}, \epsilon_{YA}$	= Axial strains in the center of specimen - $\mu\text{in./in.}$
$\epsilon_{XB}, \epsilon_{YB}$	= Bending strains in the center of specimen - $\mu\text{in./in.}$
$\epsilon_{BM1}, \epsilon_{BM2}$	= Strain in the center of the specimen, determined by small deflection beam theory and large deflection beam theory, respectively, $\mu\text{in./in.}$
ϵ_{PL}	= Strain in the center of the specimen determined by plate theory - $\mu\text{in./in.}$

LIST OF SYMBOLS, continued

ϕ	= Integration variable in the elliptic integral - $\sin^{-1}[(\sin\theta/2)/p]$
ψ, ψ_1, ψ_2	= Slopes of the four-point beam at a general point, loading point B, and at the tip, C - rad.
ψ_0	= Complementary angle of the end slope, $\psi_2 - 90 - \psi_2$, rad.
λ_0	= Complementary angle of the slope ψ_1 at the loading point B - $90 - \psi_1$, rad.
ν	= Poisson's ratio
σ_x, σ_y	= Normal components of stress parallel to x- and y-axes, psi.
τ_{xy}	= Shearing stress component in x-y coordinates, psi.
θ	= A variable used in the large deflection beam theory - $\psi + \psi_0$, rad.

SECTION 1

INTRODUCTION

1.1 BACKGROUND INFORMATION

The projection moiré method has been used successfully to determine the out-of-plane motions of large surfaces experiencing a dynamic response to an impulsive load (References 1 and 2). This method will perform equally well in situations where the response of the test specimen is static. Use of this moiré method permits the motion of the test specimen to be determined without physical contact between the test specimen and the device. If, then, surface strains can be computed from the out-of-plane moiré deformations of a test object, the projection moiré method would become an economical, noncontact experimental tool in the stress analysis of complicated structural shapes.

Determination of the surface strains from the surface deflection data presents some problems because of error magnification that results from using inexact experimental data to compute the second derivatives. Various numerical curve fitting methods have been used to obtain the higher order derivatives. Among these, the three methods used most successfully are spline functions (References 3 to 7), beam functions (Reference 8), and least square regression analysis (Reference 9).

1.2 PROGRAM OBJECTIVE AND SUMMARY

The primary objective of this program was to determine surface strains on flat plate specimens experiencing static loads from out-of-plane deformations obtained with use of the projection moiré method. To accomplish this, a four-point bending test specimen, in conjunction with a four-point bending load device, was selected as a target since a fairly uniform strain field exists in the midsection of the loaded specimen. A conventional method of strain measurement was chosen to provide data for comparison with the calculated moiré strains. For this purpose,

a number of electrical resistance strain gages were installed on the test specimen and strain measurements made for each load condition.

Theoretical strains were also determined to aid in the evaluation. The small-deflection beam theory was the only analytical method which permitted deflections and strains in the four-point bending specimen to be predicted directly. Therefore, a large-deflection beam theory which integrates the Bernoulli-Euler beam equations by use of elliptic integrals (References 10 and 11) and a small-deflection plate theory which integrates the Lagrange plate equation by use of a series of trigonometric functions (Reference 12) were developed for use with the four-point bending specimen. The moiré deflections and strains were compared with the analytically predicted deflections and strains, with the experimentally determined strains from the electrical gages, and with deflections from dial gages.

SECTION 2

EXPERIMENTAL TECHNIQUES

A brief description of the four-point bending test fixture test specimen, moiré device, and strain gage instrumentation is given in the following paragraphs. The tests performed during this program are summarized later in this section.

2.1 TEST SPECIMEN

The test specimen, shown in Figure 1, was a 26-inch long, 6-inch wide, 0.25-inch thick flat plate made of 2024-T351 aluminum alloy. One side of the plate was prepared for recording moiré fringes by the application of a reflective coating and installation of fiducial marks as illustrated in Figure 2.

2.2 FOUR-POINT BENDING LOAD DEVICE

A four-point bending load device generally consists of two knife-edge or cylindrical supports on which a beam can be simply supported at its ends and two loading points equidistant from the end supports. When loaded this way, a constant bending moment is generated in the beam between the loading points.

The four-point bending load device designed and fabricated for this investigation is shown in Figure 2. This fixture has several unique features. The beam is supported by the inner loading points and the loads are applied to the ends of the beam by means of finely threaded power screws. The loading points which come in contact with the test specimen are four ground cylindrical rods, 3/4 inches in diameter and 6 inches long. The loading points in the ends are guided so that the applied loads are parallel to each other and normal to the surface of the test specimen. Load cells incorporated in the inner loading points were calibrated prior to their use. Loads, i.e., analog voltages, were read on separate digital voltmeters to an accuracy of ± 0.01 volts or ± 0.5 pounds. Loads were accurately balanced, controlled, and

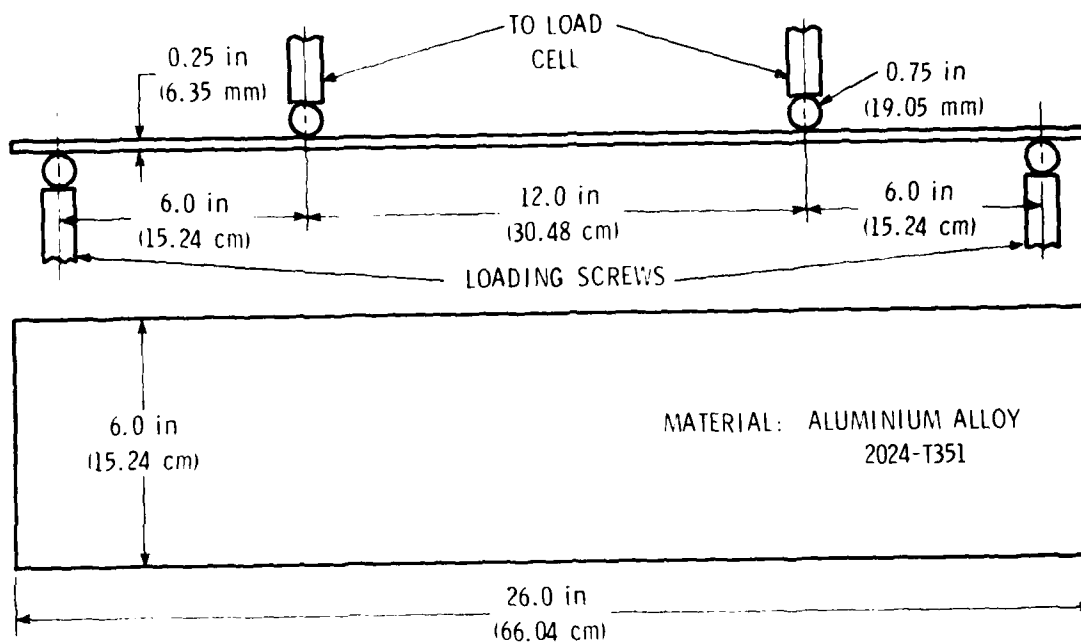


Figure 1. Four-Point Bending Specimen.

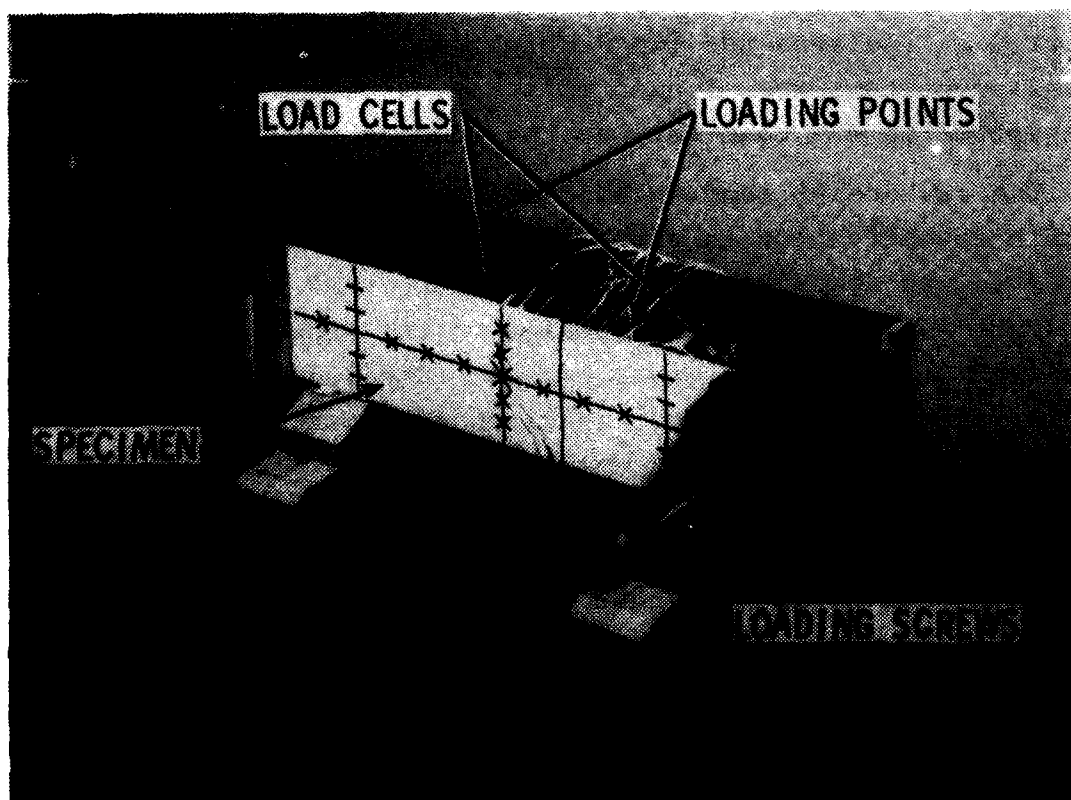


Figure 2. Four-Point Bending Load Device.

applied by turning the power screws and monitoring the loads on the load cells.

2.3 INSTRUMENTATION

The moire device used in this investigation is described in Reference 1. For reader convenience, the basic experimental setup is shown in Figures 3 and 4.

Four Micro-Measurements EA-13-250BF-350 strain gages were installed in the center and back-to-back on the front and rear surfaces of the test specimens in the x and y directions so that they measured the ϵ_x and ϵ_y strains (Figure 5). These strain gage circuits were balanced on a 10-channel Vishay bridge balance and were read on a Vishay strain meter.

A dial indicator gage whose sensitivity is 0.001 inch was used to measure the deflections at the center of the plate.

2.4 . MATRIX FOR EXPERIMENTAL INVESTIGATIONS

The experimental effort conducted in support of the program objective is summarized in Table 1.

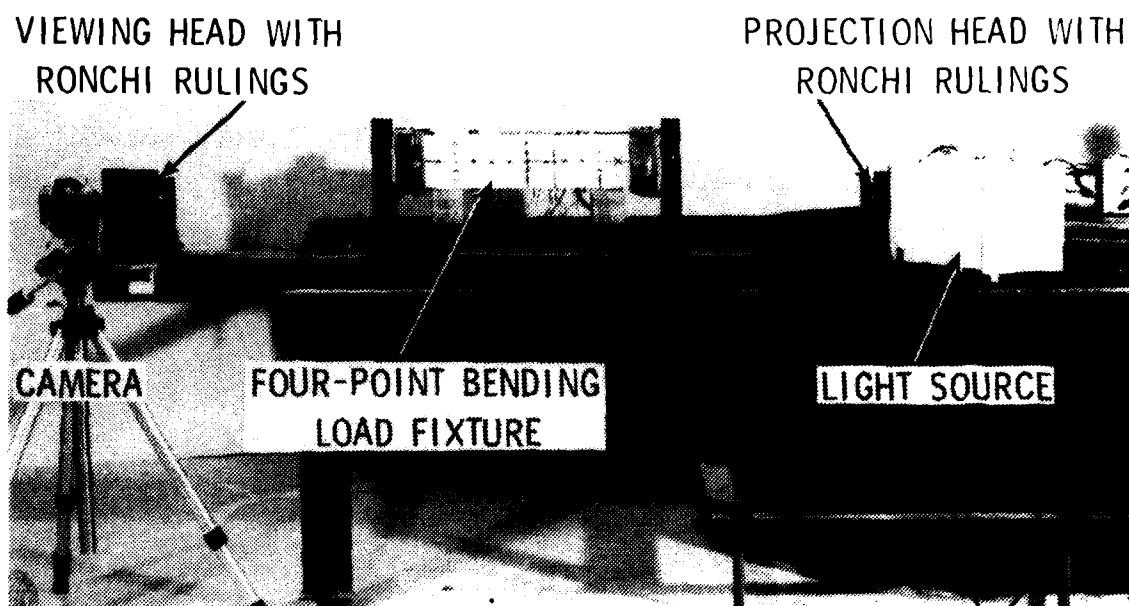


Figure 3. Moire Device with Four-Point Bending Load Fixture.

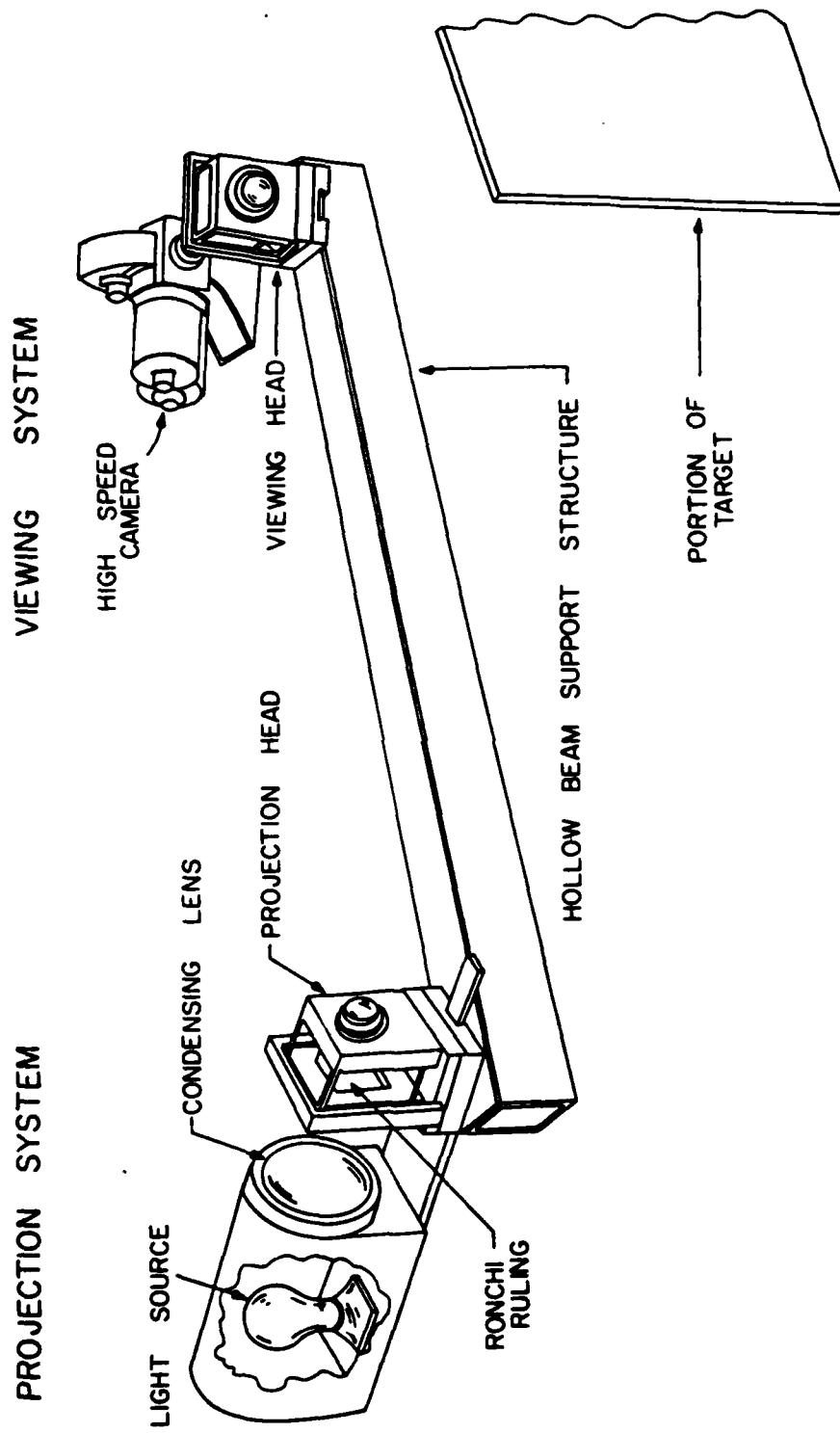


Figure 4. Schematic View of Moiré Device Illustrating Components and their Relationship to Target.

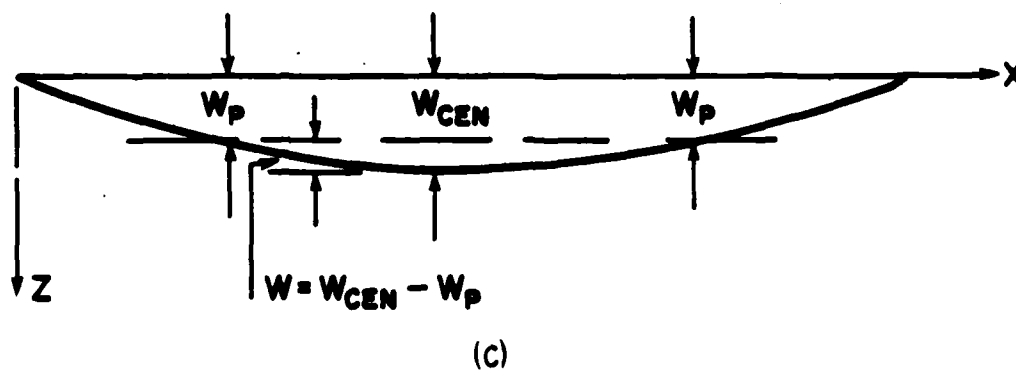
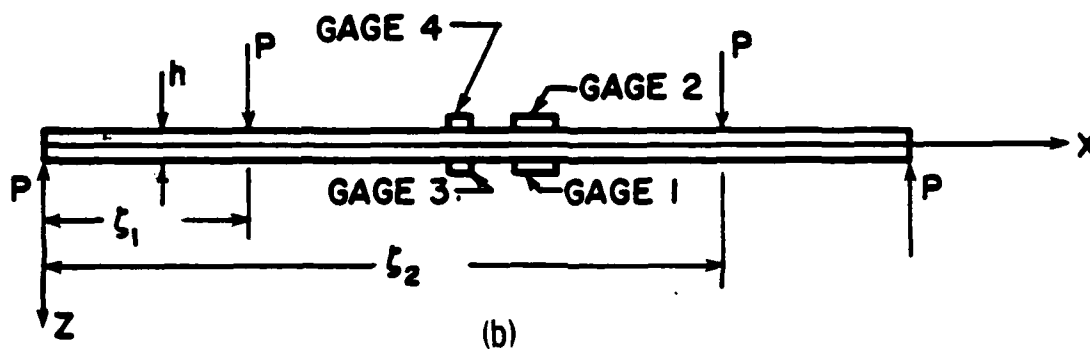
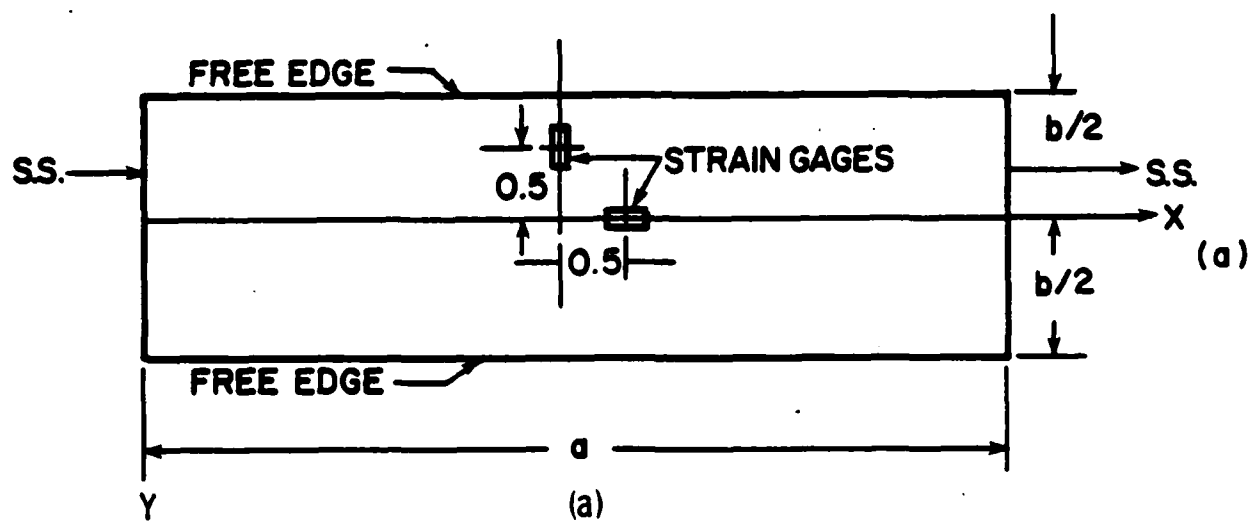


Figure 5. Four-Point Bending Plate Specimen.

TABLE 1

TEST MATRIX

TEST SERIES		Load (lbs)						
		5	55	105	155	205	255	305
I Ronchi Ruling Lines Vertical	Moire Fringe Exposures	2	2	2	2	2	2	2
	Strain Gage Readings	1	1	1	1	1	1	1
II Ronchi Ruling Lines Horizontal	Moire Fringe Exposures	2	2	2	2	2	2	2
	Strain Gage Readings	1	1	1	1	1	1	1
III Dial Gage Readings	Increases in Loading Sequence	1	1	1	1	1	1	1
	Decreases in Loading Sequence	1	1	1	1	1	1	1

SECTION 3

ANALYTICAL TECHNIQUES

The test specimen was subjected to a range of loads which would induce both small and large deflections. Hence, it was necessary to predict the static response of the test specimen by both small and large deflection theories. A brief outline of the theories used and the solutions obtained are given in the following paragraphs.

3.1 SMALL-DEFLECTION PLATE THEORY

The Lagrange plate equation is given by (Reference 12)

$$\frac{\partial^4 w}{\partial x^4} + 2 \frac{\partial^4 w}{\partial x^2 \partial y^2} + \frac{\partial^4 w}{\partial y^4} = \frac{q}{D} \quad (1)$$

The simple support boundary conditions are

$$w = 0, \quad \frac{\partial^2 w}{\partial x^2} = 0 \text{ for } x = 0 \text{ and } x = a \quad (2)$$

The free-edge boundary conditions are

$$\left(\frac{\partial^2 w}{\partial y^2} + \nu \frac{\partial^2 w}{\partial x^2} \right) = 0 \text{ for } y = \pm b/2 \quad (3)$$

$$\left(\frac{\partial^3 w}{\partial y^3} + (2-\nu) \frac{\partial^3 w}{\partial x^2 \partial y^2} \right) = 0 \text{ for } y = \pm b/2 \quad (4)$$

The deflected surface is assumed in the form of a series (Figure 5)

$$w = w_1 + w_2 \quad (5)$$

where

$$w_1 = \frac{2Pa^3}{\pi^4 bD} \sum_{m=1,3,5}^{\infty} \sum_{j=1}^2 \frac{1}{m^4} \sin \frac{m\pi \zeta_j}{a} \cdot \sin \frac{m\pi x}{a} \quad (6)$$

represents the deflection curve of a four-point bending strip,
and

$$w_2 = \frac{Pa^3}{\pi^4 bD} \sum_{m=1,3,5}^{\infty} \left\{ A_m \cosh \frac{m\pi y}{a} + B_m \frac{m\pi y}{a} \sinh \frac{m\pi y}{a} \right\} \sin \frac{m\pi x}{a} \quad (7)$$

A_m and B_m are determined from the boundary conditions (2), (3), and (4) and are represented by

$$A_m = \frac{2\nu}{m^4} \frac{(1-\nu) \cosh \alpha_m - (1+\nu) \sinh \alpha_m}{(\nu^2 + 2\nu - 3) \sinh \alpha_m \cosh \alpha_m + (1-\nu)^2 \alpha_m^2} \sum_{j=1}^2 \sin \frac{m\pi \zeta_j}{a} \quad (8)$$

$$B_m = \frac{2\nu}{m^4} \frac{-(1-\nu) \sinh \alpha_m}{(\nu^2 + 2\nu - 3) \sinh \alpha_m \cosh \alpha_m + (1-\nu)^2 \alpha_m^2} \sum_{j=1}^2 \sin \frac{m\pi \zeta_j}{a} \quad (9)$$

This series solution converges very rapidly. The first three terms are sufficient for deflections and the first six terms should be considered for stresses. The details of the analytical expressions are given in Appendix A.

3.2 LARGE-DEFLECTION BEAM THEORY

By symmetry the beam is considered to be fixed at A and only one half of the beam is shown (Figure 6). The Bernoulli-Euler equations for the beam in the regions BC and AB are given by

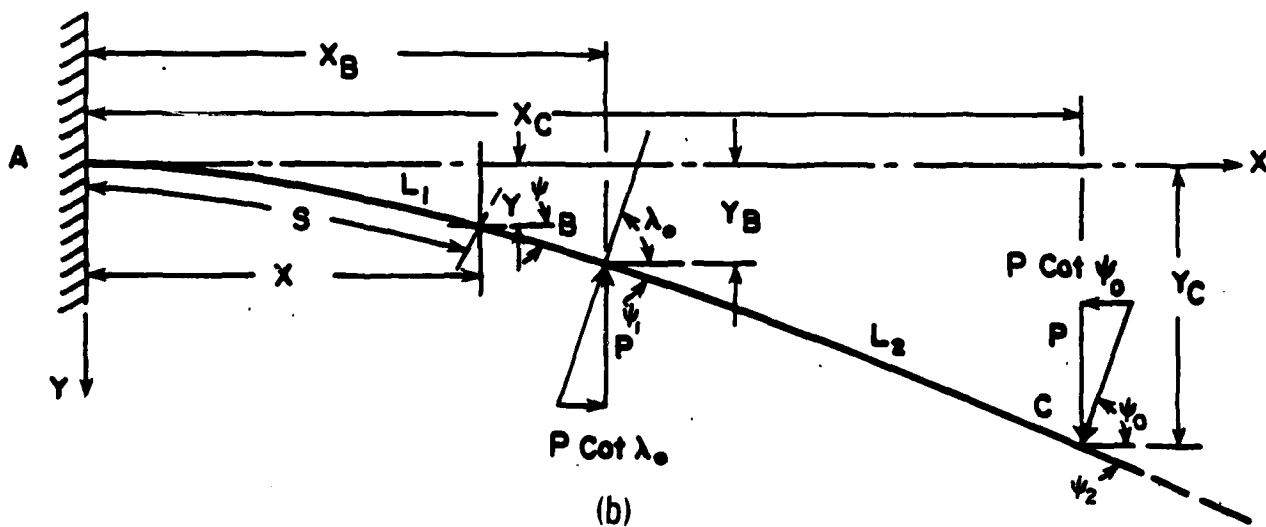
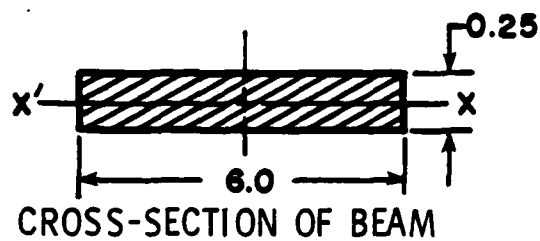
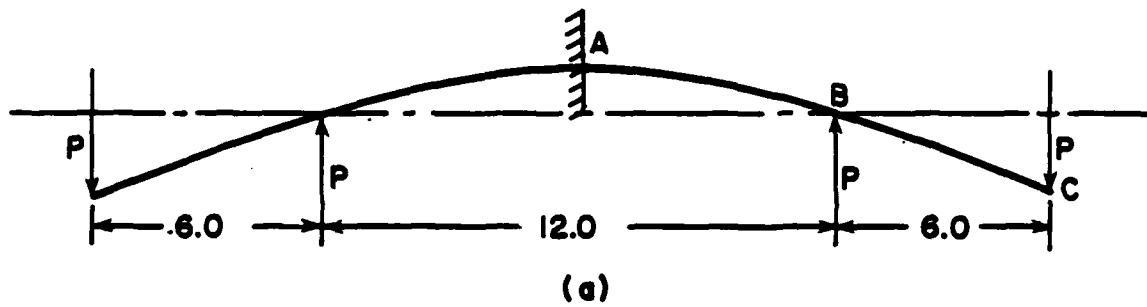


Figure 6. Four-Point Bending Beam Specimen.

$$D \frac{d\psi}{ds} = P(x_C - x) + P \cot \psi_0 (y_C - y) \text{ for } x_C > x > x_B \quad (10)$$

$$D \frac{d\psi}{ds} = P(x_C - x) + P \cot \psi_0 (y_C - y) - P(x_B - x) - P \cot \lambda_0 (y_B - y) \text{ for } x_B > x \geq 0 \quad (11)$$

The boundary conditions are

$$\left[\frac{d\psi}{ds} \right]_{\psi=\psi_2} = 0 \quad (12)$$

$$[\psi]_{s=0} = 0 \quad (13)$$

$$\left[\frac{d\psi}{ds} \right]_{\psi=\psi_1} \text{ to be continuous} \quad (14)$$

These differential equations (10) and (11) are integrated and the constants of integration are determined from the boundary conditions (12), (13), and (14). The equations for L_1 , L_2 , x_B , y_B , x_C , and y_C are expressed in terms of elliptic integrals of the first and second kind and are given below. The details of the derivation are given in Appendix B.

$$L_1 = \frac{1}{k_1} K(p_1, N) \quad (15)$$

$$L_2 = \frac{1}{k_2} [K(p) - k(p, \bar{m})] \quad (16)$$

$$y_B = \frac{2p_1}{k_1} [1 - \cos N] \quad (17)$$

$$y_C = y_B + \frac{1}{k_2} \{-\sin \psi_0 [K(p, m) - K(p) + 2E(p) - 2E(p, m)] + 2p \cos \psi_0 \cos m\} \quad (18)$$

$$x_B = \frac{1}{k_1} [3K(p_1, N) - 2E(p_1, N)] \quad (19)$$

$$x_C = x_B + \frac{1}{k_2} \{ \cos \psi_0 [K(p, \bar{m}) - K(p) + 2E(p) - 2E(p, \bar{m})] + 2p \sin \psi_0 \cos \bar{m} \} \quad (20)$$

where

$$K(\bar{m}) = \int_0^{\pi/2} \frac{d\phi}{\sqrt{1-p^2 \sin^2 \phi}}$$

$$E(\bar{m}) = \int_0^{\pi/2} \sqrt{1-p^2 \sin^2 \phi} d\phi$$

are complete elliptic integrals of first and second kind, and

$$K(p, \bar{m}) = \int_0^{\bar{m}} \frac{d\phi}{\sqrt{1-p^2 \sin^2 \phi}}$$

$$E(p, \bar{m}) = \int_0^{\bar{m}} \sqrt{1-p^2 \sin^2 \phi} d\phi$$

are elliptic integrals of first and second kind.

$$p = \sin \pi/4 \quad (21)$$

$$p_1 = \frac{1}{\sqrt{2}} \sqrt{\left\{ 1 - \cos \psi_1 + \frac{k_2^2}{k_1^2} [\cos(\pi/2 + \psi_1 - \psi_2)] \right\}} \quad (22)$$

$$k_1 = \sqrt{\left\{ \frac{p}{D} (\cot \psi_0 - \cot \lambda_0) \right\}} \quad (23)$$

$$k_2 = \sqrt{\frac{P}{D \sin \psi_0}} \quad (24)$$

$$\bar{m} = \sin^{-1} \left[\frac{\sin \frac{\psi_1 + \psi_0}{2}}{p} \right] \quad (25)$$

$$N = \sin^{-1} \left[\frac{\sin \psi_1 / 2}{p_1} \right] \quad (26)$$

A numerical solution of these equations for a four-point bending test specimen is obtained by applying the condition that the supports are a known distance apart and the length of the beam can change during loading (References 10 and 11). This condition is imposed by the use of Equations 19 and 20. A value for ψ_2 is assumed and Equation 20 is solved for \bar{m} . The value of ψ_1 is then obtained from Equation 25 and the value of K_1 , p_1 and N are then computed from Equations 23, 22, and 26 and substituted into Equation 19. This numerical iteration is continued and a set of values for ψ_1 and ψ_2 are finally obtained after a few trials to simultaneously satisfy Equations 19 and 20.

SECTION 4

EXPERIMENTAL AND ANALYTICAL RESULTS

A brief description of the experimental procedure and the moiré, the strain gage, and the dial gage results are given in the following paragraphs. The analytical results are presented and compared with experimental results.

4.1 EXPERIMENTAL PROCEDURE

The total number of tests were organized into three separate categories, e.g., Test Series I, II, and III, as shown in Table 1. In Test Series I, the moiré device was held horizontally thereby projecting vertical Ronchi rulings. A preload of five pounds was applied to the specimen to firmly position the specimen against the supports. The strain gages were zeroed and the reference moiré fringes were recorded. Loads were applied to the specimen in increments of 50 pounds to a maximum load of 305 pounds. At each increment of load, two photographs of the moiré fringe pattern were taken, and the meter readings were scanned manually and recorded.

In Test Series II, the moiré device was rotated 90° so that horizontal Ronchi rulings were projected onto the test specimen. The moiré fringes and strains from strain gages were recorded by the procedures outlined for Test Series I.

In Test Series III, a dial gage was positioned to measure deflection at the center of the specimen. A preload of five pounds was applied to the specimen to firmly position the specimen against the supports, and the initial reading of the dial gage was recorded. Loads were then applied to the specimen in increments of 50 pounds to a maximum load of 305 pounds and then decreased by 50 pound increments to the initial five-pound preload. Dial gage readings were noted at each increment or decrement of applied load. The deflection at each load was obtained as the difference between the dial gage reading at that load and the preload.

4.2 MOIRE RESULTS

The test specimen was considered to be a plate with curvatures $\frac{\partial^2 w}{\partial x^2}$ and $\frac{\partial^2 w}{\partial y^2}$ in the x and y directions. The moiré device was used to determine these curvatures. The moiré device was held in the horizontal position to determine $\frac{\partial^2 w}{\partial x^2}$ and in the vertical position to determine $\frac{\partial^2 w}{\partial y^2}$. Moiré fringe patterns for these cases are shown in Figures 7 and 8. Deflected shapes of the loaded plates were computed using measurements taken from the photographs and a program called STRAIN. Deflection data were fitted to quadratic and cubic polynomials using a least-square curve fitting routine called LSQ. Slopes and curvatures of the deflected shapes were determined using a program called PLATE. The moiré strains are given from the relations

$$\epsilon_x = -z \left(\frac{\partial^2 w}{\partial x^2} \right) \quad (27)$$

$$\epsilon_y = -z \left(\frac{\partial^2 w}{\partial y^2} \right) \quad (28)$$

In the case of large deflections, the curvatures are replaced by the expression

$$\frac{1}{R_x} = - \frac{\frac{\partial^2 w}{\partial x^2}}{\left[1 + \left(\frac{\partial w}{\partial x} \right)^2 \right]^{3/2}} \quad (29)$$

$$\frac{1}{R_y} = - \frac{\frac{\partial^2 w}{\partial y^2}}{\left[1 + \left(\frac{\partial w}{\partial x} \right)^2 \right]^{3/2}} \quad (30)$$



(a) 5 POUNDS LOAD



(b) 55 POUNDS LOAD



(c) 105 POUNDS LOAD

Figure 7. Moiré Fringes to Determine $\frac{\partial^2 w}{\partial x^2}$ Curvature.



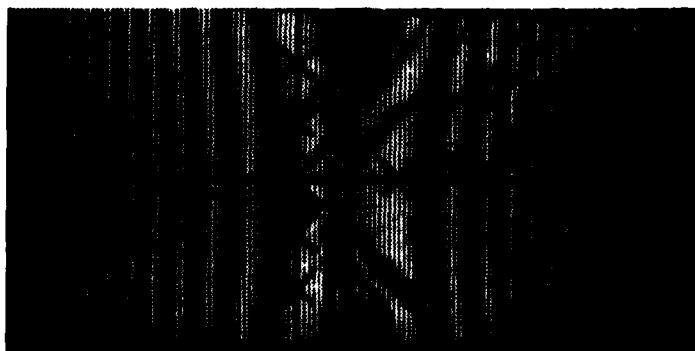
(d) 155 POUNDS LOAD



(e) 205 POUNDS LOAD



(f) 255 POUNDS LOAD



(g) 305 POUNDS LOAD

Figure 7. (Cont.)



(a) 5 POUNDS LOAD



(b) 55 POUNDS LOAD



(c) 105 POUNDS LOAD

Figure 8. Moiré Fringes to Determine $\frac{\delta_w^2}{\delta y^2}$ Curvature.



(d) 155 POUNDS LOAD



(e) 205 POUNDS LOAD



(f) 255 POUNDS LOAD



(g) 305 POUNDS LOAD

Figure 8. (Concluded)

The $\frac{\partial^2 w}{\partial y^2}$ curvature of the four-point bending test specimen is a small quantity compared to $\frac{\partial^2 w}{\partial x^2}$, and the very small number of moiré fringes are insufficient to accurately determine this quantity. Therefore, according to References 13, 14, and 15, $\frac{\partial^2 w}{\partial y^2}$ curvature is assumed to be $-\nu \frac{\partial^2 w}{\partial x^2}$ and the strain ϵ_y is given by

$$\epsilon_y = -\nu \frac{\partial^2 w}{\partial x^2} = -\nu \epsilon_x \quad (31)$$

The $\frac{\partial^2 w}{\partial y^2}$ curvatures are also determined directly from Figure 8 for a few load cases.

The moiré deflections and strains are presented for loads of 50 to 300 pounds in Tables 2 and 3, and in Figures 9 and 10. The moiré deflections computed by program STRAIN were fit to a second order polynomial using the least squares routine PLSCF and a second order Legendre polynomial, and the experimental points and the fitted curves were plotted using plot routine PLOTS, Figures 11 and 12.

The scatter of moiré experimental data is large at small loads and the experimental data points cannot be fit by means of a polynomial. It should be remembered that the plate specimen has initial imperfections which are of the same order of magnitude as the deflections corresponding to these smaller loads. This could be the cause for the large amount of scatter. At higher loads, the moiré experimental points can easily be fitted by means of second or third degree polynomials and the experimental scatter is greatly reduced.

4.3 DEFLECTIONS FROM DIAL GAGES

The deflections measured by dial gages are given in Table 4 and shown previously in Figure 9.

TABLE 2
MOIRÉ DEFLECTIONS AND STRAINS
AT THE BEAM CENTER

Load (lbs)	Deflections W (in)	Strain (μ)	
		ϵ_x	ϵ_y
50	0.045	385.3* (363.64)†	-128.44 (-121.22)
100	0.094	765.84 (766.34)	-255.28 (-255.46)
150	0.144	1185.90 (1186.66)	-394.9 (-394.9)
200	0.193	1599.18 (1602.68)	-533.06 (-534.22)
250	0.251	1987.76 (2005.52)	-662.58 (-668.52)
300	0.300	2347.38 (2398.84)	-782.46 (-818.30)

*Quadratic polynomial curve-fit

†Cubic polynomial curve-fit

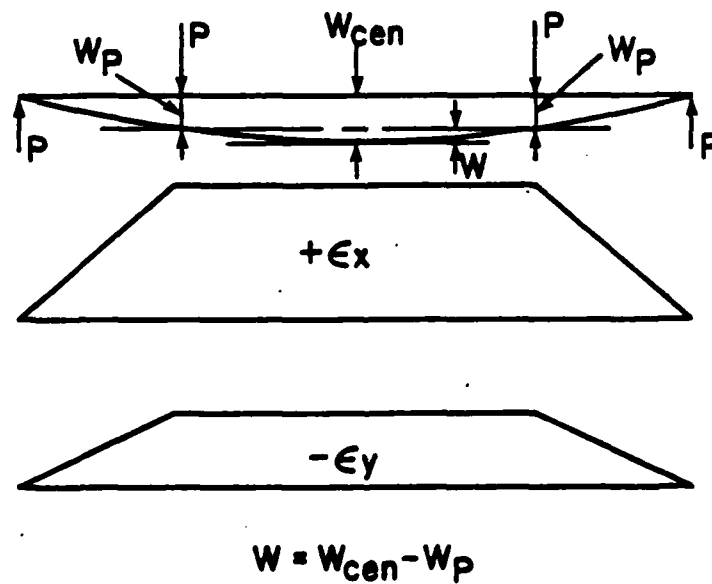
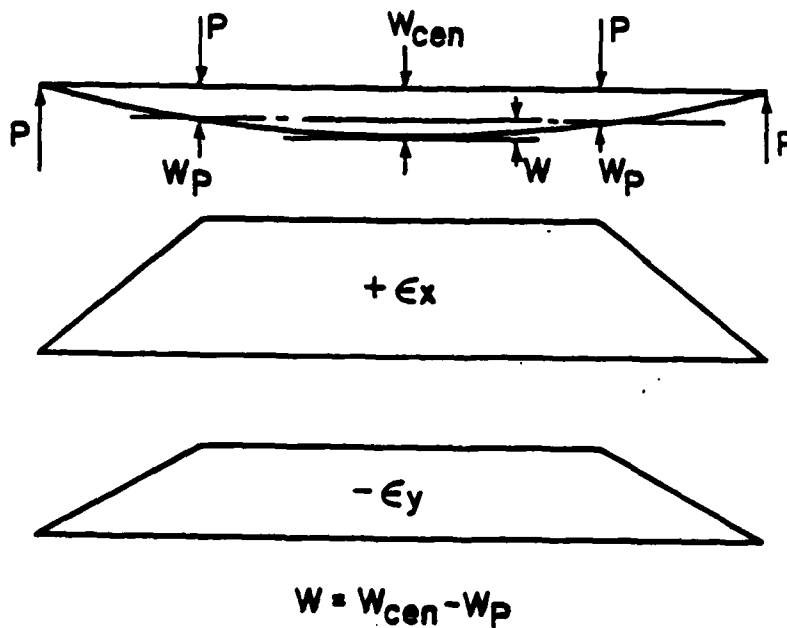


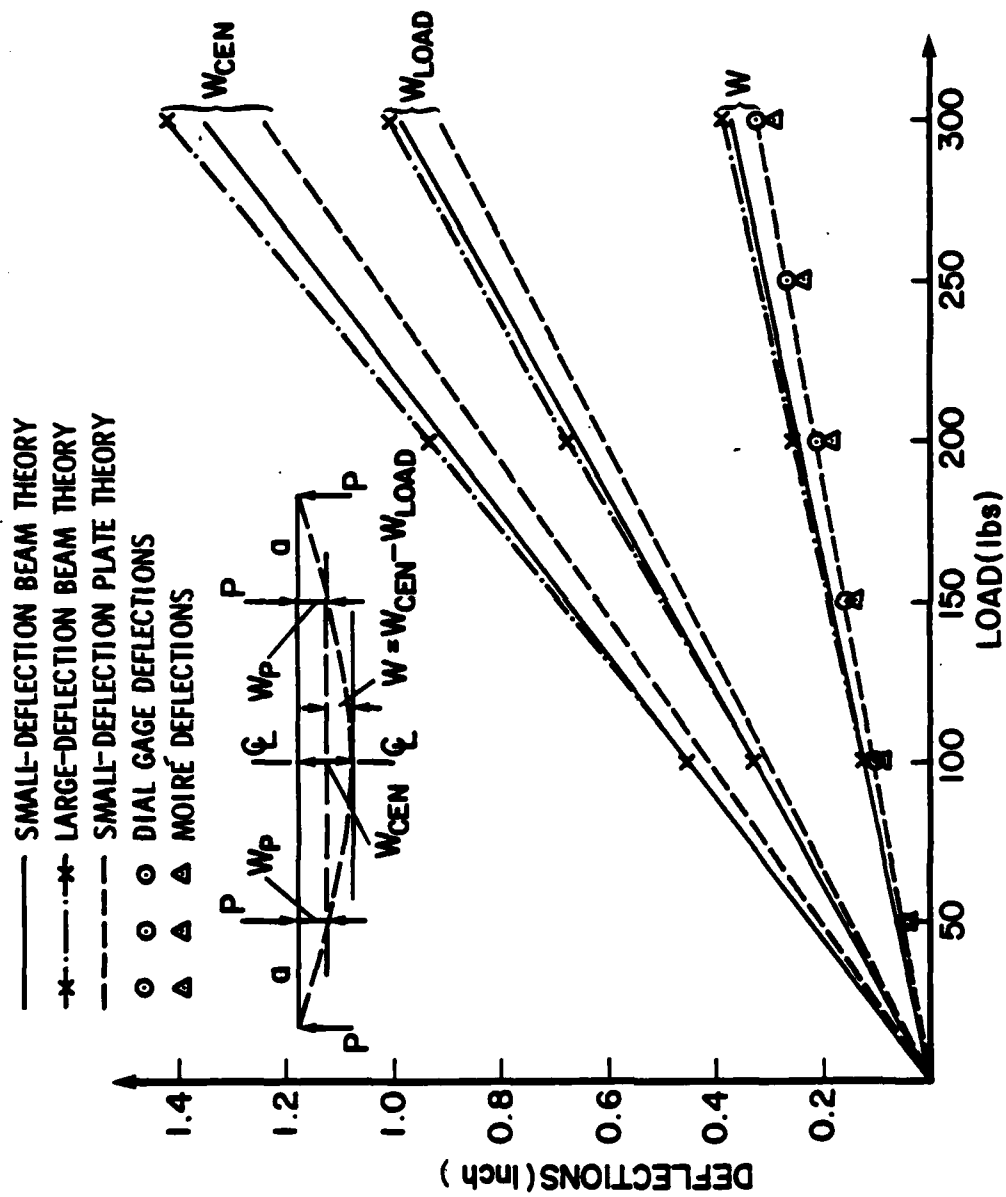
TABLE 3
MOIRÉ DEFLECTIONS AND STRAINS
THREE INCHES BELOW CENTER

Load (lbs)	Deflection w (in)	Strain (μ)	
		ϵ_x	ϵ_y
50	0.061	465.38*	-155.12
		(455.3)†	(-151.76)
100	0.099	719.76	-239.52
		(718.56)	(-239.52)
150	0.147	1166.5	-388.82
		(1161.9)	(-387.3)
200	0.193	1542.78	-514.24
		(1537.32)	(-512.44)
250	0.252	1981.46	-660.5
		(2005.54)	(-668.52)
300	0.304	2347.38	-784.32
		(2406.96)	(-802.32)

*Quadratic polynomial curve-fit

†Cubic polynomial curve-fit





NOTE: Limit of accuracy on moiré data is 0.01 inches.

Figure 9. Comparison of Experimental and Analytical Deflections.

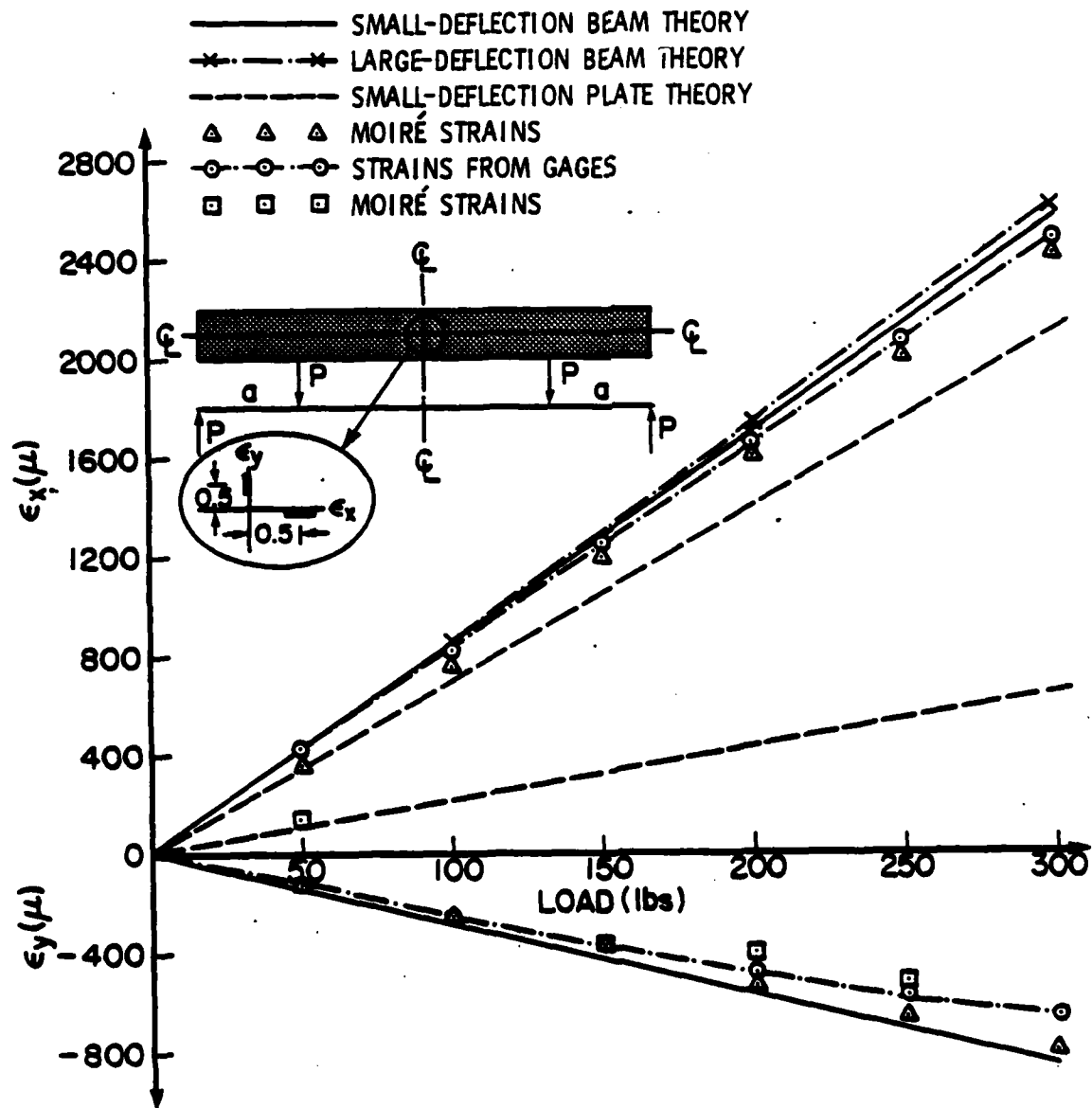
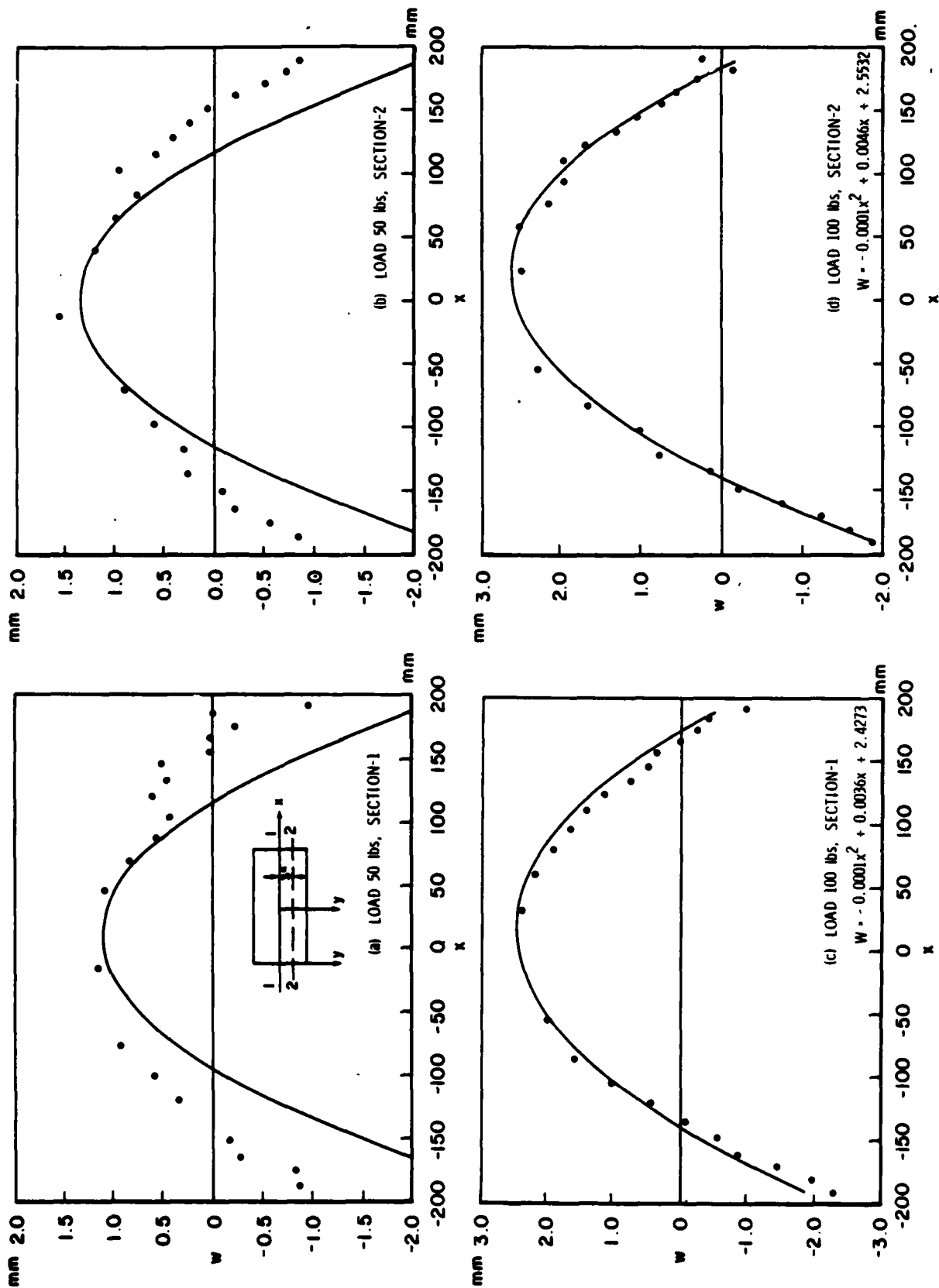
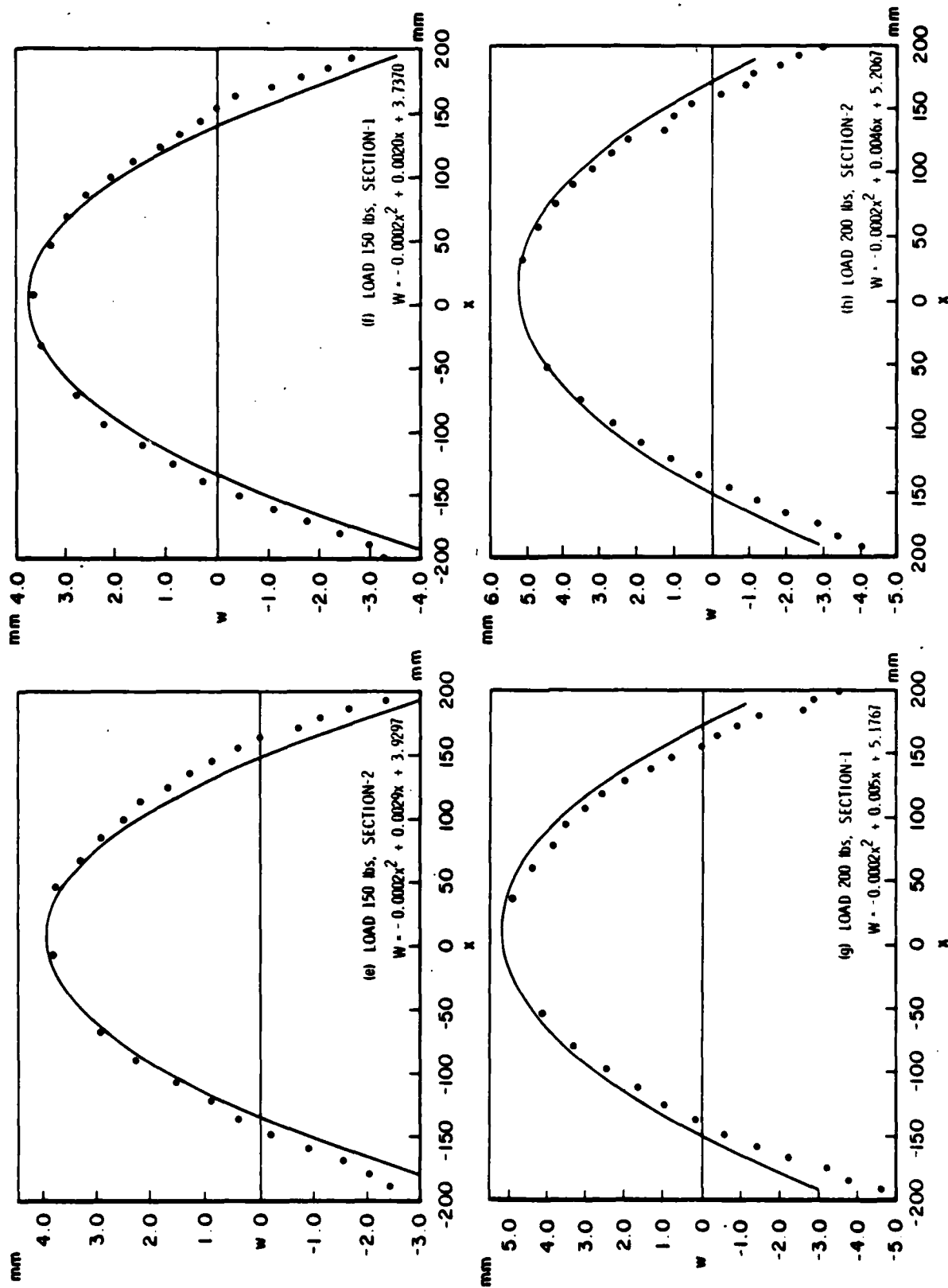


Figure 10. Comparison of Experimental and Analytical Strains.



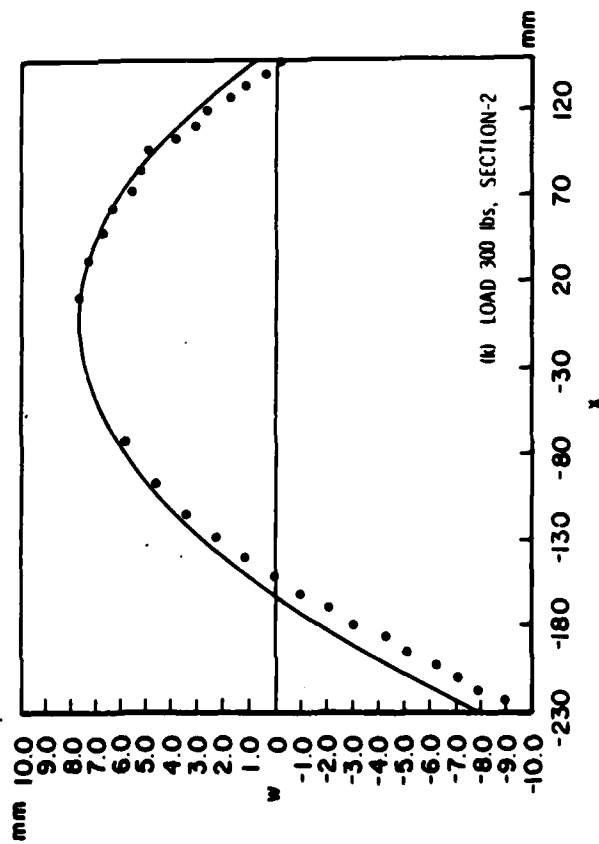
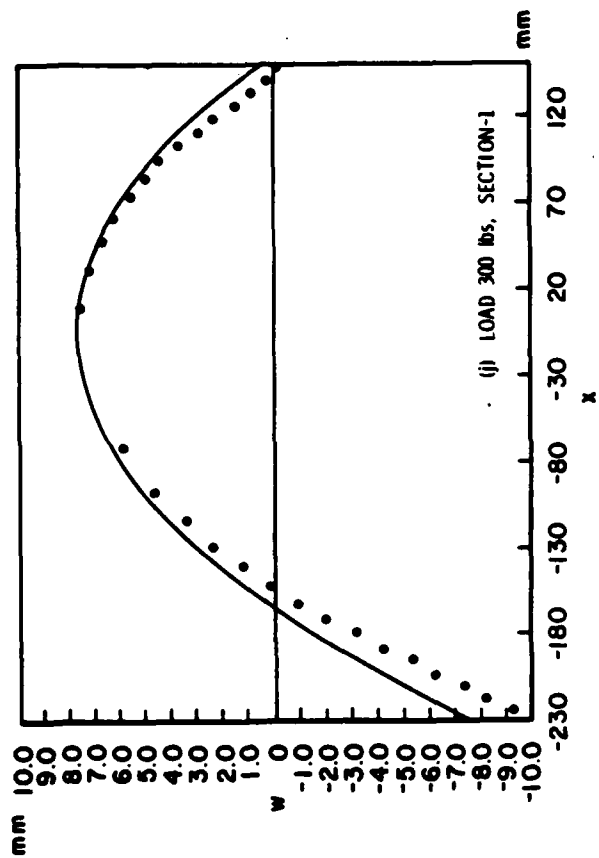
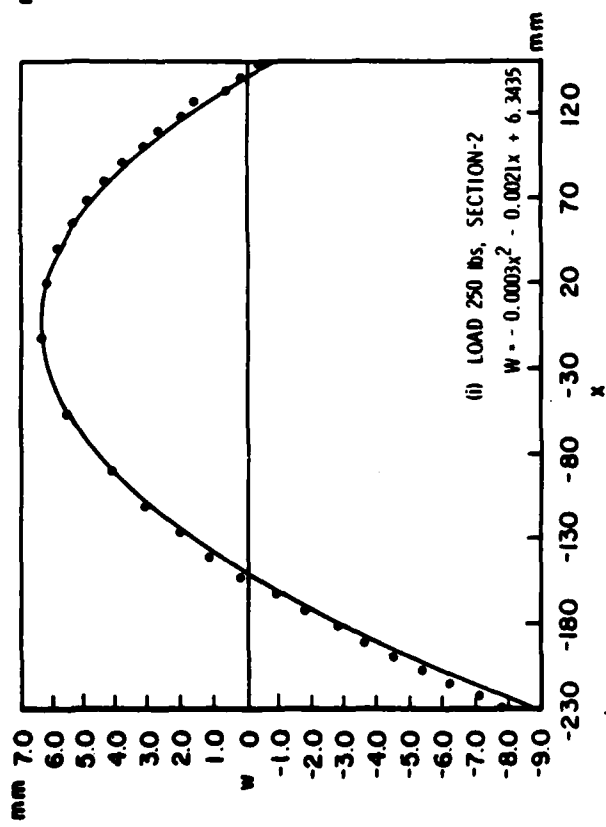
NOTE: Limit of accuracy on moiré data is 0.25mm

Figure 11. Regression Analysis Using a Second-Order Polynomial Relating Deflections and Span Positions.



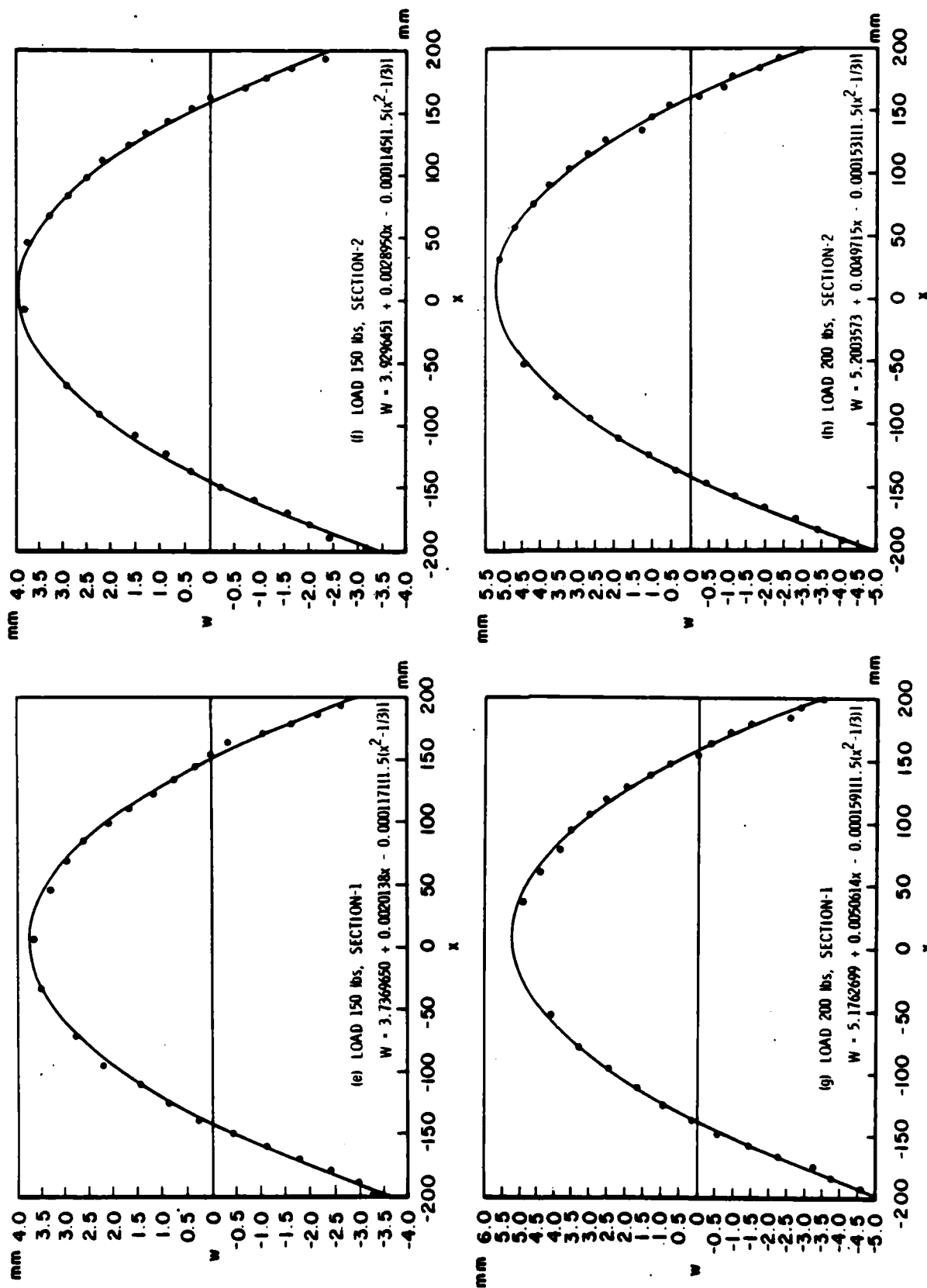
NOTE: Limit of accuracy on moiré data is 0.25mm

Figure 11. (Continued)



NOTE: Limit of accuracy on moiré data is 0.25mm

Figure 11. (Concluded)



NOTE: Limit of accuracy on moiré data is 0.25mm

Figure 12. Regression Analysis Using a Second-Order Legendre Polynomial Relating Deflections and Span Positions.

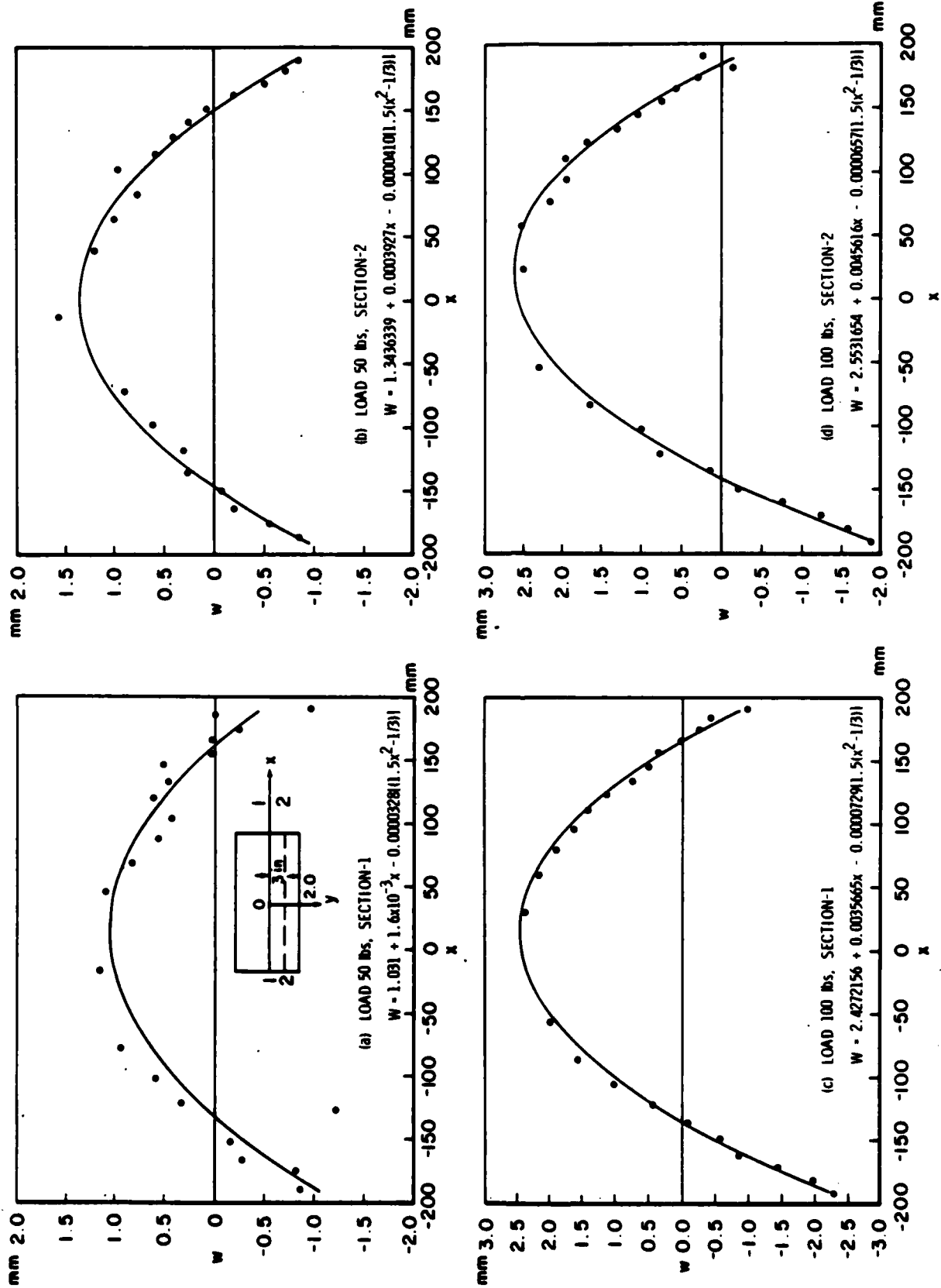
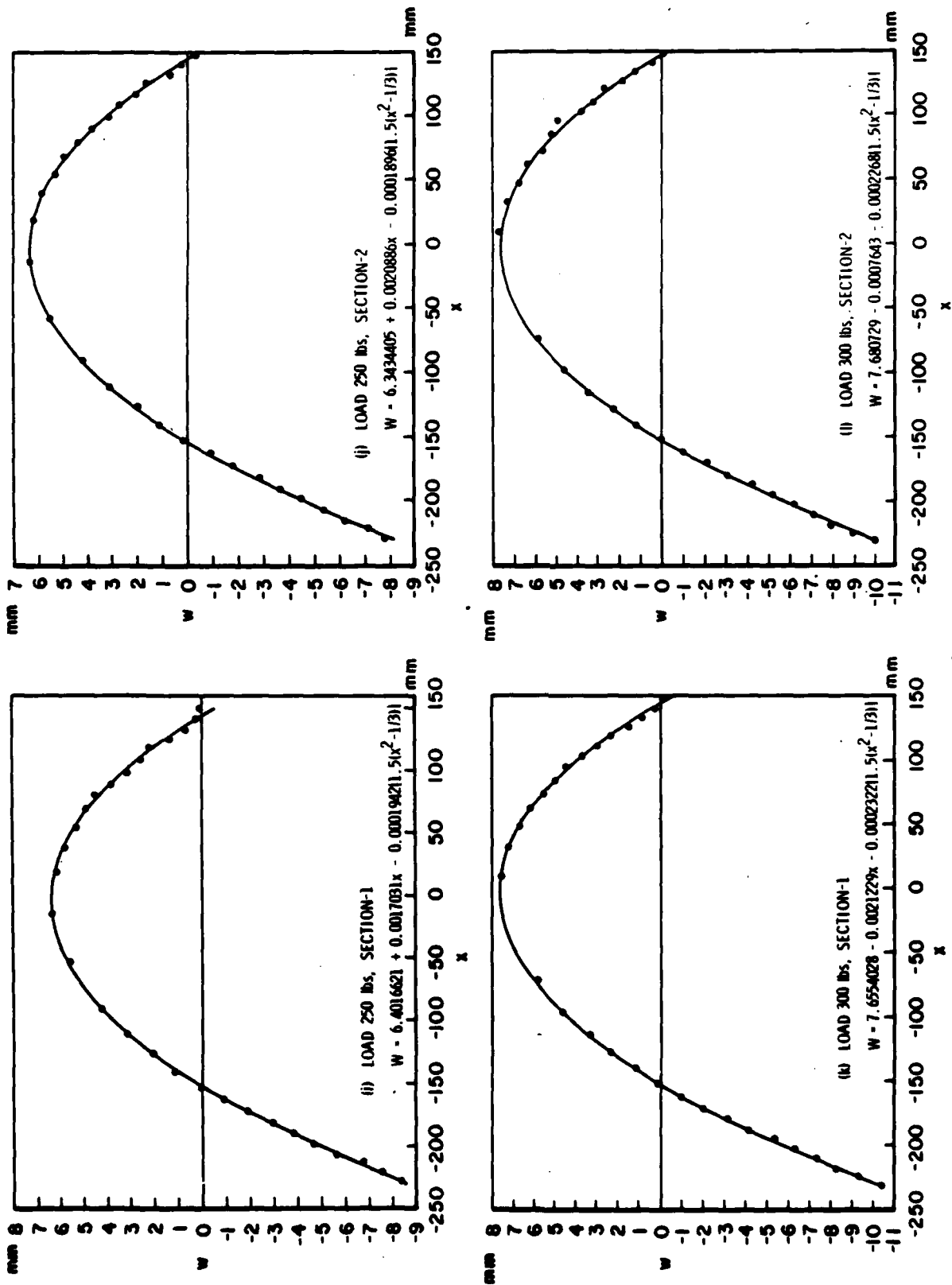


Figure 12. (Continued)

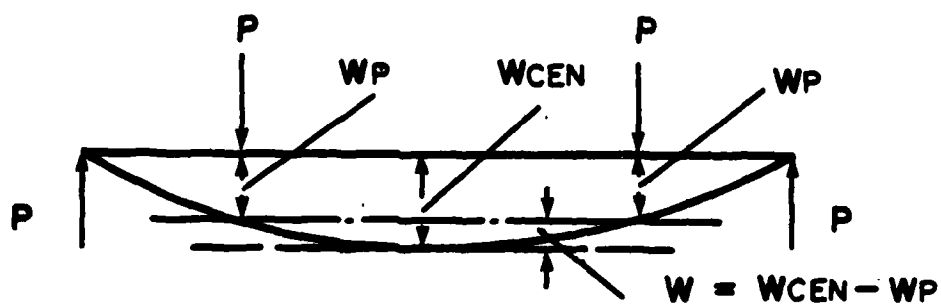


NOTE: Limit of accuracy on moiré data is 0.25mm

Figure 12. (Concluded)

TABLE 4
DIAL GAGE DEFLECTIONS AT CENTER OF BEAM

Load (lbs)	Deflections (in)
50	0.052
100	0.1055
150	0.1590
200	0.212
250	0.266
300	0.322



4.4 STRAINS FROM ELECTRICAL RESISTANCE GAGES

The strains recorded from strain gages are presented in Table 5 and shown previously in Figure 10.

4.5 ANALYTICAL RESULTS

The deflections and strains predicted from the small-deflection beam theory are presented in Table 6; from the small-deflection plate theory in Table 7; and from large-deflection beam theory in Table 8.

TABLE 5
STRAINS FROM RESISTANCE STRAIN GAGES

Load (lbs)	Gage-1 ϵ_{x1} (μ)	Gage-2 ϵ_{x2} (μ)	$\epsilon_{xB} =$ $\left(\frac{\epsilon_{x1} - \epsilon_{x2}}{2} \right)$	$\epsilon_{xA} =$ $\frac{\epsilon_{x1} + \epsilon_{x2}}{2}$	Gage-3 ϵ_{y1} (μ)	Gage-4 ϵ_{y2} (μ)	$\epsilon_{yB} =$ $\frac{\epsilon_{y1} - \epsilon_{y2}}{2}$	$\epsilon_{yA} =$ $\frac{\epsilon_{y1} + \epsilon_{y2}}{2}$	Gage Characteristics
50	+420	-424	± 422	-2	-120	+128	± 124	+4	MM: EA-13- 250BF-350 GF: 2.11 Ω : 350
100	+823	-842	± 832.50	-9.6	-237	+252	± 244.5	+7.5	
150	+1220	-1276	± 1248	-28	-350	+373	± 361.5	+11.5	
200	+1611	-1715	± 1663	-52	-450	+490	± 470	+20	
250	+1990	-2162	± 2076	-86	-540	+594	± 567	+27	
300	+2365	-2595	± 2480	-115	-610	+683	± 646.5	+36.5	

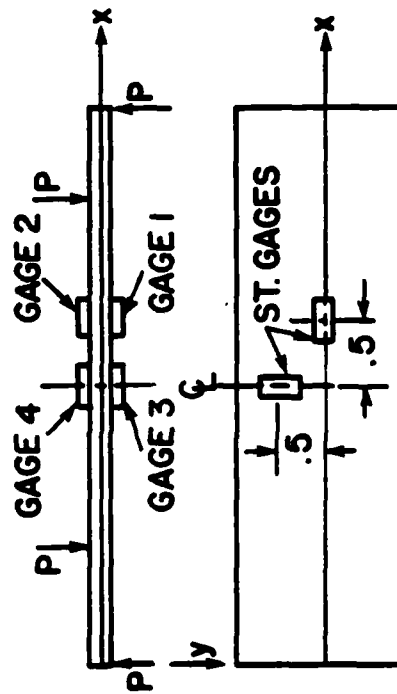
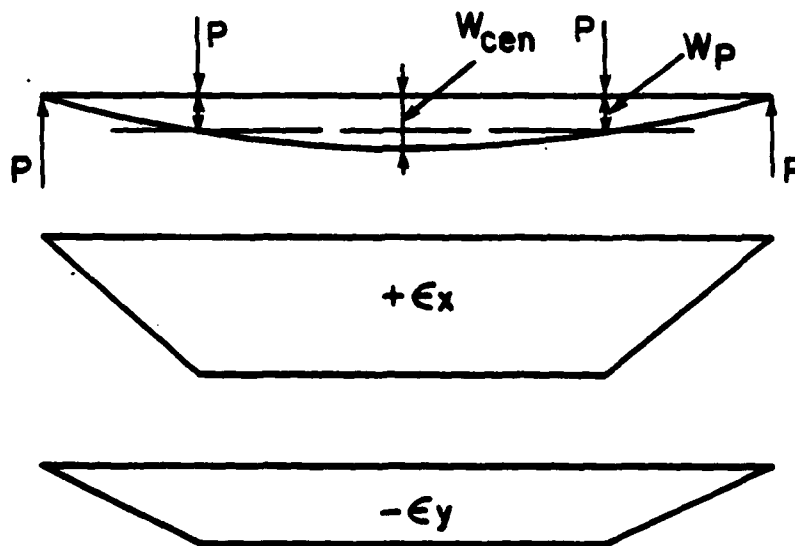


TABLE 6
DEFLECTIONS AND STRAINS FROM SMALL-DEFLECTION BEAM THEORY

Load (lb)	W_{LOAD} (in)	W_{CEN} (in)	W (in)	ϵ_x Strain μ	ϵ_x Strain μ
50	0.1638	.2253	.0615	427	-142.33
100	0.3277	.4506	.1229	853	-284.33
150	0.4915	.6759	.1844	1280	-426.67
200	0.6554	.9012	.2458	1707	-569
250	0.8192	1.1265	.3073	2133	-711
300	0.9830	1.3518	.3688	2560	-853.33



$$W = W_{cen} - W_p$$

TABLE 7

DEFLECTIONS AND STRAINS FROM SMALL-DEFLECTION PLATE THEORY

Load W	W_{Load} inch	W_{CEN} inch	W inch	ϵ_x Strain μ	ϵ_y Strain μ
50	0.1522	0.2064	0.0542	346	109
100	0.3045	0.4129	0.1083	693	217
150	0.4567	0.6193	0.1626	1040	326
200	0.6090	0.8257	0.2168	1386	435
250	0.7612	1.0322	0.2710	1733	543
300	0.9135	1.2386	0.3252	2080	652

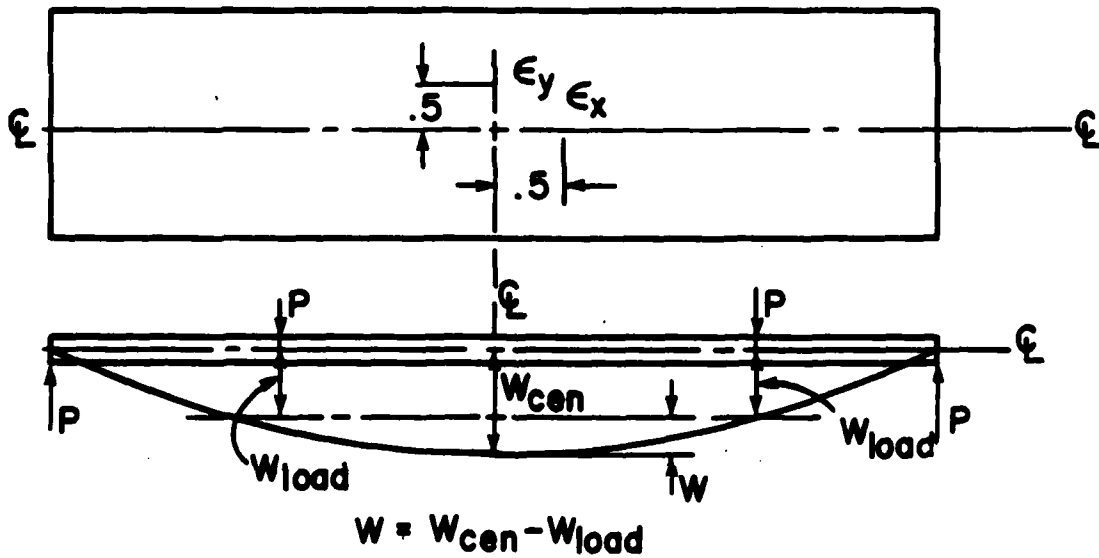
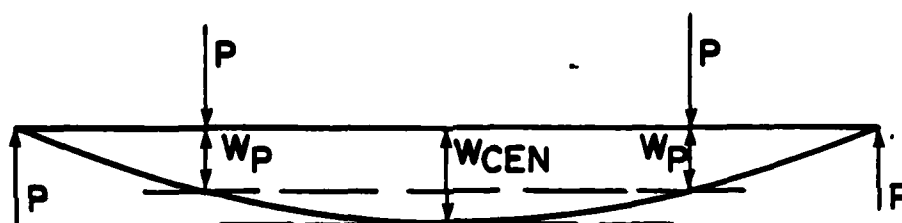
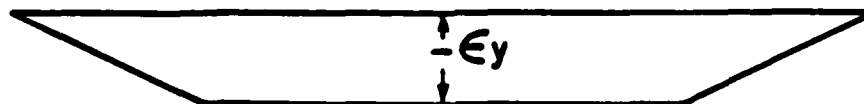
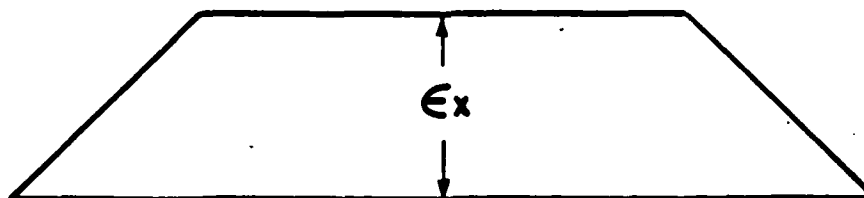


TABLE 3
DEFLECTIONS AND STRAINS BY LARGE-DEFLECTION BEAM THEORY

Load W	W_{Load} inch	W_{CEN} inch	W inch	ϵ_x Strain μ	ϵ_y Strain μ
100	0.3330	0.4577	0.1247	855	-285
200	0.6760	0.9308	0.2547	1724	-575
300	1.0351	1.4182	0.3830	2621	-874



$$W = W_{\text{CEN}} - W_P$$



SECTION 5

ANALYSIS OF RESULTS

Deflections are compared in Figure 9 and in Table 9, and strains are compared in Figure 10 and in Tables 10, 11, and 12. The deflections from dial gages and strains from resistance gages are considered as standards with which the deflections and strains by other methods are compared and evaluated.

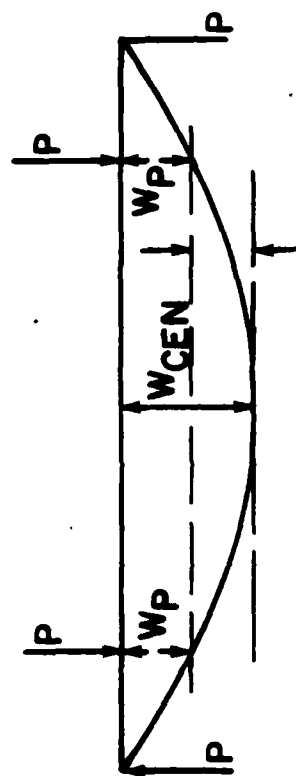
In comparison with the dial gage deflections, the moiré deflections are smaller by 7 to 13 percent; deflections predicted by small-deflection plate theory are higher by 1 to 4 percent; the large-deflection beam theory deflections are higher by 18 to 20 percent; and small-deflection beam theory deflections are higher by 15 to 18 percent. Thus the small-deflection plate theory predicts deflections in close agreement to the dial gage deflections. The deflections determined by the moiré fringe technique are more accurate at higher loads. This is due to initial imperfections of the test specimen which will be of the same order of magnitude as the deflections at small loads. This causes considerable scatter of the experimental data points as seen in Figures 11 and 12. At higher loads, when the deflections are large, the scatter in experimental data points is reduced and moiré deflections agree within 6 percent with dial gage deflections. Another cause for the large discrepancy noticed between moiré and dial gage deflections was due to the fact that the initial reference surface was not perfectly flat, as most machined flat plates have some initial imperfections. The test specimens were prepared from rolled plate and developed imperfections during machining which could not be easily removed.

In comparison with resistance strain gage strains, the moiré ϵ_x strains computed by second and third order polynomials are smaller by 0 to 8 percent (Table 10 and Figure 10), whereas those computed by Legendre polynomials are smaller by 6 to 25 percent (Table 11); the classical beam theory ϵ_x strains are

TABLE 9

COMPARISON OF DEFLECTIONS:
MOIRÉ, DIAL GAGE, BEAM THEORIES AND PLATE THEORY

Load	Dial Gage	Moiré	$\frac{W_M - W_D}{W_D} \times 100$	Plate Theory	$\frac{W_{PL} - W_D}{W_D} \times 100$	Large-Deflection Beam	$\frac{W_{LBM} - W_D}{W_D} \times 100$	Classical Beam Theory	$\frac{W_{BM} - W_D}{W_D} \times 100$
(lbs)	W_D	W_M		W_{PL}		W_{LBM}		W_{BM}	
50	0.0520	0.0453	-12.88	0.0542	+4.23			0.0615	18.26
100	0.1055	0.0940	-10.90	0.1083	+2.65	0.1247	18.20	0.1229	16.49
150	0.1590	0.1441	-9.37	0.1626	+2.26			0.1844	15.97
200	0.212	0.1932	-8.87	0.2168	+2.26	0.2547	20.14	0.2468	15.94
250	0.266	0.2510	-5.64	0.2710	+1.88			0.3073	15.52
300	0.322	0.3000	-6.83	0.3252	+0.99	0.3830	18.94	0.3688	14.53



$$W = W_{CEN} - W_P$$

TABLE 10

COMPARISONS OF ϵ_x STRAINS: MOIRÉ, RESISTANCE GAGES, BEAM THEORIES, PLATE THEORY

Load (lbs)	Strain Gage ϵ_{x1}	Moiré Strain ϵ_{xM}^*	$\frac{\epsilon_{xM} - \epsilon_{x1}}{\epsilon_{x1}} \times 100$	Small- Deflection Beam Theory ϵ_x (BM1)	$\frac{\epsilon_x \text{ (BM1)} - \epsilon_{x1}}{\epsilon_{x1}} \times 100$	Large- Deflection Beam Theory ϵ_x (BM2)	$\frac{\epsilon_x \text{ (BM2)} - \epsilon_{x1}}{\epsilon_{x1}} \times 100$	Plate Theory ϵ_x (PL)	$\frac{\epsilon_x \text{ (PL)} - \epsilon_{x1}}{\epsilon_{x1}} \times 100$
50	420	385.3	-8.26	427	1.42			346	-18.01
100	823	765.84	-6.95	853	2.52	855	2.7	693	-16.76
150	1220	1185.9	-2.80	1280	2.56			1040	-16.67
200	1611	1559.18	-0.74	1707	2.65	1724	3.67	1386	-16.66
250	1990	1987.76	-0.11	2133	2.75			1733	-16.52
300	2365	2347.38	-0.75	2560	3.23	2621	5.69	2080	-16.13

*Curve fit by second and third order polynomials.

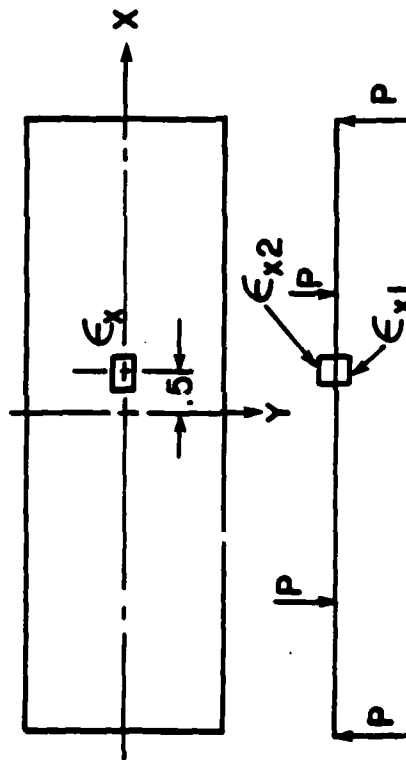


TABLE 11

COMPARISON OF MOIRÉ STRAINS (BY LEGENDRE POLYNOMIALS) WITH RESISTANCE GAGES

Load (lbs)	Resistance Gages		Moiré Strains					
			Section AA			Section BB		
	ϵ_{x1}	ϵ_{y1}	ϵ_{xM}^{\dagger}	$\frac{\epsilon_{xM} - \epsilon_{x1}}{\epsilon_{x1}} \times 100$	ϵ_{yM}^{\dagger}	$\frac{\epsilon_{yM} - \epsilon_{y1}}{\epsilon_{y1}} \times 100$	ϵ_{xM}^{\dagger}	ϵ_{yM}^{\dagger}
50	420	-120	312.42	-25.61	-104.14	-13.22	390.53	-130.18
100	823	-237	694.37	-15.62	-231.46	- 2.34	625.79	-208.59
150	1220	-350	1115.38	- 8.58	-371.80	+ 6.23	1090.61	-363.54
200	1611	-450	1515.43	- 5.93	-505.13	+12.25	1458.28	-486.09
250	1990	-540	1849.76	- 7.05	-616.48	+14.16	1805.94	-601.98
300	2365	-610	2211.71	- 6.48	-737.24	+20.86	2160.27	-720.09

†Curve fit by second order Legendre polynomial

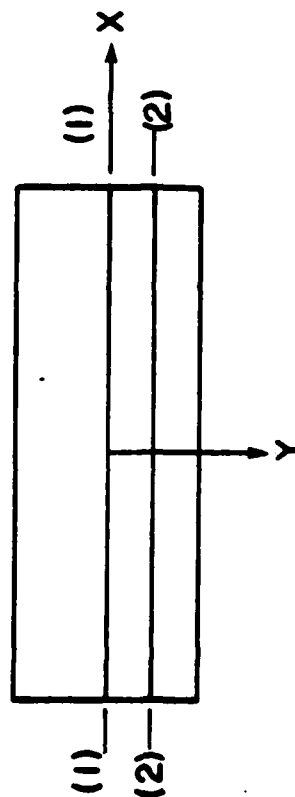
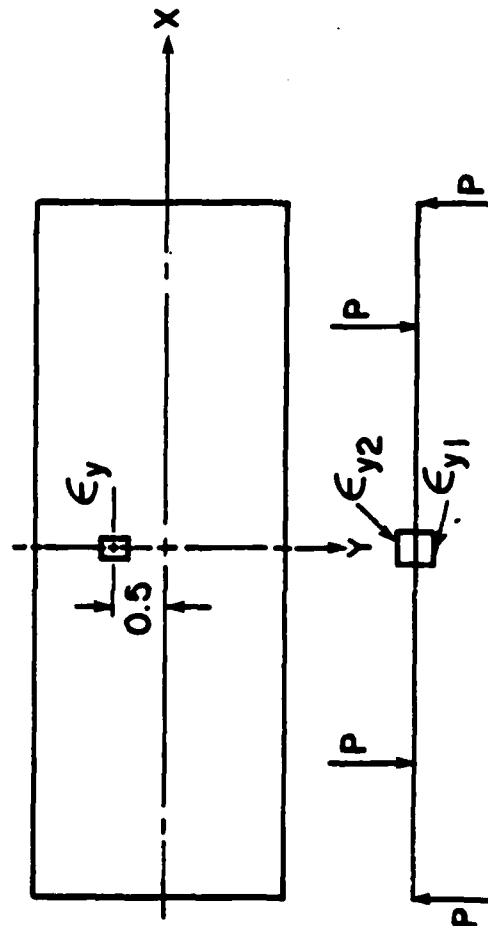


TABLE 12

COMPARISON OF ϵ_y STRAINS: MOIRÉ, RESISTANCE GAGES, BEAM THEORIES, PLATE THEORY

Load (lbs)	Strain Gage ϵ_{y1}	Moiré Strain (First Method) ϵ_{yM1}	Moiré Strain (Second Method) ϵ_{yM2}	$\frac{\epsilon_{yM1} - \epsilon_{y1}}{\epsilon_{y1}} \times 100$	$\frac{\epsilon_{yM2} - \epsilon_{y1}}{\epsilon_{y1}} \times 100$	Small- Deflection Beam Theory ϵ_{yBM1}	$\frac{\epsilon_{yBM1} - \epsilon_{y1}}{\epsilon_{y1}} \times 100$	Large- Deflection Beam Theory ϵ_{yBM2}	$\frac{\epsilon_{yBM2} - \epsilon_{y1}}{\epsilon_{y1}} \times 100$	Plate Theory $\epsilon_{y(PL)}$
50	-120	-128.44		7.03	-	-142	+14.52			109
100	-237	-255.28		7.71	-	-284.33	+16.29	-285	+16.56	217
150	-350	-394.9	-349.16	12.83	0.24	-426.67	+18.03			326
200	-450	-533.06	-413.91	18.46	8.02	-569.00	+21.07	-575	+22.30	435
250	-540	-668.52	-531.91	23.80	1.50	-711.00	+25.40			543
300	-610	-818.30		34.15	-	-853.33	+31.99	-874	+35.19	652



higher by 1.5 to 3 percent; the large-deflection beam theory ϵ_x strains are higher by 3 to 6 percent; the ϵ_x strains from classical plate theory are smaller by 16 to 18 percent. Thus the moiré ϵ_x strains computed by second and third order polynomials are in close agreement with resistance gage strains, especially at higher loads, and can be predicted by small-deflection beam theory over the range of loads considered in this investigation.

The moiré ϵ_y strains were determined by two methods. In the first method, since the curvature in the y-direction is (References 13, 14, and 15):

$$\frac{\partial^2 w}{\partial y^2} = -\nu \frac{\partial^2 w}{\partial x^2} ,$$

the ϵ_y strain can be approximated by

$$\epsilon_y = -\nu \epsilon_x .$$

In the second method, $\frac{\partial^2 w}{\partial y^2}$ curvature is determined directly from the Moiré fringe photographs of Figure 8. The ϵ_y strains obtained by the first method are compared in Tables 11 and 12 and in Figure 10. In comparison with resistance gage strains, the ϵ_y moiré strains obtained by second and third order polynomials are higher by 7 to 34 percent; whereas those obtained by a second-order Legendre polynomial are higher by 6 to 20 percent; the small-deflection beam theory ϵ_y strains are higher by 15 to 32 percent; the large-deflection beam theory ϵ_y strains are higher by 17 to 35 percent. Classical plate theory predicts tensile ϵ_y strains and cannot be compared with resistance gage strains. The solution strategy used in the classical plate theory is similar to the one used by Timoshenko for many of the plate bending problems. But this strategy may not give true solutions due to the type of loading, boundary conditions, and possibly due to the large aspect (a/b) ratio of 4 of the test specimen. The ϵ_y moiré strains determined by the second method for loads of 150, 200, and 250

pounds are compared in Figure 10 and these are smaller than resistance gage strains by 0 to 8 percent. Therefore, none of the analytical methods considered in this investigation predict the ϵ_y strains accurately. The ϵ_y Moiré strain determined by the second method is closer to resistance gage strains and therefore is to be preferred to the first method.

For the loads considered in this investigation, curvatures determined by large deflection equations (Equations 29 and 30) did not differ significantly from the curvatures determined by small deflections and therefore the numerical results are not presented for these.

SECTION 6

CONCLUSIONS AND RECOMMENDATIONS

The following conclusions are based on the results of this program.

1. The projection moiré method used in this investigation determines both the deflections and strains accurately in flat surfaces undergoing large deformations due to static loads. However, the strains determined by regression analysis using second and third order polynomials and second order Legendre polynomials are accurate only for the center portion of the beam.

2. Of the analytical methods, small-deflection beam theory and large-deflection beam theory predicted beam deflections and ϵ_x strain accurately. Plate theory predicted the deflections very accurately. The ϵ_y strains were not predicted accurately by any of the methods investigated.

The following recommendations are made. (1) Other numerical curve fitting methods such as spline approximations and beam functions should be tried to obtain accurate second derivatives from the moiré deformations at any position along the span of the beam. (2) The investigations reported herein should be extended to evaluate the accuracy of the method for curved surfaces under dynamic response conditions.

APPENDIX A

SMALL DEFLECTION PLATE THEORY FOR FOUR-POINT BENDING PLATE SPECIMEN

BASIC EQUATIONS

The Lagrange plate equation is given by

$$\frac{\partial^4 w}{\partial x^4} + 2 \frac{\partial^4 w}{\partial x^2 \partial y^2} + \frac{\partial^4 w}{\partial y^4} = \frac{q}{D} \quad (A-1)$$

where w is the downward deflection, q is the intensity of the load and D is given by $\frac{Eh^3}{12(1-\nu^2)}$. The boundary conditions are

$$w = 0 ; \quad \frac{\partial^2 w}{\partial x^2} = 0 \quad \text{for } x = 0, \text{ and } a \quad (A-2)$$

$$\left(\frac{\partial^2 w}{\partial y^2} + \nu \frac{\partial^2 w}{\partial x^2} \right) = 0 \quad \text{for } y = \pm b/2 \quad (A-3)$$

$$\left(\frac{\partial^3 w}{\partial y^3} + (2-\nu) \frac{\partial^3 w}{\partial x^2 \partial y} \right) = 0 \quad \text{for } y = \pm b/2 \quad (A-4)$$

The load is symmetrical with respect to the x -axis (Figure 4) and therefore the deflection surface is symmetrical with respect to x -axis. Therefore we can consider only the conditions along the side $y = +b/2$.

The deflection surface is assumed in the form

$$w = w_1 + w_2 \quad (A-5)$$

where

$$w_1 = \frac{2Pa^3}{\pi^4 bD} \sum_{m=1,3,5}^{\infty} \sum_{j=1}^2 \frac{1}{m^4} \sin \frac{m\pi c_j}{a} \cdot \sin \frac{m\pi x}{a} \quad (A-6)$$

$$w_2 = \frac{Pa^3}{\pi^4 bD} \sum_{m=1,3,5}^{\infty} \left(A_m \cosh \frac{m\pi y}{a} + B_m \frac{m\pi y}{a} \cdot \sinh \frac{m\pi y}{a} \right) \sin \frac{m\pi x}{a} \quad (A-7)$$

The constants A_m and B_m are given by

$$A_m = \frac{2v}{m^4} \frac{(1-v) \cosh \alpha_m - (1+v) \sinh \alpha_m}{(v^2 + 2v - 3) \sinh \alpha_m \cosh \alpha_m + (1-v)^2 \alpha_m} \cdot \sum_{j=1}^2 \sin \left(\frac{m\pi c_j}{a} \right) \quad (A-8)$$

$$B_m = \frac{2v}{m^4} \frac{-(1-v) \sinh \alpha_m}{(v^2 + 2v - 3) \sinh \alpha_m \cosh \alpha_m + (1-v)^2 \alpha_m} \cdot \sum_{j=1}^2 \sin \left(\frac{m\pi c_j}{a} \right) \quad (A-9)$$

where $\alpha_m = \frac{m\pi b}{a}$

The moment-curvature relations are given by

$$M_x = -\bar{D} \left[\frac{\partial^2 w}{\partial x^2} + v \frac{\partial^2 w}{\partial y^2} \right] \quad (A-10)$$

$$M_y = -\bar{D} \left[\frac{\partial^2 w}{\partial y^2} + v \frac{\partial^2 w}{\partial x^2} \right] \quad (A-11)$$

$$M_{xy} = \bar{D}(1-v) \frac{\partial^2 w}{\partial x \partial y} \quad (A-12)$$

The maximum stresses at the surface of the plate are given by

$$\sigma_x = \pm \frac{6M_x}{h^2} \quad (A-13)$$

$$\sigma_y = \pm \frac{6M_y}{h^2} \quad (A-14)$$

$$\tau_{xy} = \tau_{yx} = \pm \frac{3M_{xy}}{h^2} \quad (A-15)$$

The maximum strains at the surfaces of the plate are given by

$$\epsilon_x = \mp z \frac{\partial^2 w}{\partial x^2} = \mp \frac{h}{2} \cdot \frac{\partial^2 w}{\partial x^2} \quad (A-16)$$

$$\epsilon_y = \mp z \frac{\partial^2 w}{\partial y^2} = \mp \frac{h}{2} \cdot \frac{\partial^2 w}{\partial y^2} \quad (A-17)$$

The value of the first three constants of the trigonometric series are given by

A_1	B_1	A_3	B_3	A_5	B_5
-0.21651606	+0.03558502	0.01535823	0.01942625	-0.0001234	-0.00012857

$$\sigma_x = \pm \frac{6Pa}{\pi^2 h^2 b} \sum_{m=1,3,5}^{\infty} \left[\frac{2\nu}{m^2} \left(\sin \frac{m\pi \zeta_1}{a} + \sin \frac{m\pi \zeta_2}{a} \right) + m^2 \left\{ (A_m(1-\nu) - 2\nu B_m) \cosh \frac{m\pi y}{a} + B_m(1-\nu) \cdot \frac{m\pi y}{a} \cdot \sinh \frac{m\pi y}{a} \right\} \right] \sin \frac{m\pi x}{a} \quad (A-18)$$

$$\sigma_y = \mp \frac{6Pa}{\pi^2 h^2 b} \sum_{m=1,3,5}^{\infty} \left[\frac{2\nu}{m^2} \left(\sin \frac{m\pi \zeta_1}{a} + \sin \frac{m\pi \zeta_2}{a} \right) + m^2 \left\{ (A_m(1-\nu) + 2\nu B_m) \cosh \frac{m\pi y}{a} + B_m(1-\nu) \cdot \frac{m\pi y}{a} \cdot \sinh \frac{m\pi y}{a} \right\} \right] \sin \frac{m\pi x}{a} \quad (A-19)$$

$$\tau_{xy} = \pm \frac{3Pa(1-\nu)m^2}{\pi^2 h^2 b} \sum_{m=1,3,5}^{\infty} \left[(A_m + B_m) \sinh \frac{m\pi y}{a} + B_m \cdot \frac{m\pi y}{a} \cdot \cosh \frac{m\pi y}{a} \right] \cos \frac{m\pi x}{a} \quad (A-20)$$

$$\epsilon_x = \pm \frac{6(1-\nu^2)Pa}{\pi^2 E h^2 b} \sum_{m=1,3,5}^{\infty} \left[\frac{2}{m^2} \left(\sin \frac{m\pi \zeta_1}{a} + \sin \frac{m\pi \zeta_2}{a} \right) + m^2 \left\{ A_m \cosh \frac{m\pi y}{a} + B_m \frac{m\pi y}{a} \cdot \sinh \frac{m\pi y}{a} \right\} \right] \cdot \sin \frac{m\pi x}{a} \quad (A-21)$$

$$\epsilon_y = \mp \frac{6(1-\nu^2)Pa}{\pi^2 E h^2 b} \sum_{m=1,3,5}^{\infty} m^2 \left\{ A_m \cosh \frac{m\pi y}{a} + 2B_m \cosh \frac{m\pi y}{a} + B_m \frac{m\pi y}{a} \cdot \sinh \frac{m\pi y}{a} \right\} \cdot \sin \frac{m\pi x}{a} \quad (A-22)$$

$$\gamma_{xy} = \pm \frac{3(1-\nu)Pa}{\pi^2 G h^2 b} \sum_{m=1,3,5}^{\infty} m^2 \left\{ (A_m + B_m) \sinh \frac{m\pi y}{a} + B_m \cdot \frac{m\pi y}{a} \cdot \cosh \frac{m\pi y}{a} \right\} \cdot \cos \frac{m\pi x}{a} \quad (A-23)$$

APPENDIX B

LARGE DEFLECTION BEAM THEORY FOR A FOUR-POINT BENDING BEAM SPECIMEN

BASIC EQUATIONS

Let $L = L_1 + L_2$ be the length of cantilever and $D = \frac{EI}{1-\nu^2}$ its flexural rigidity. For a point U between B and C (Figure 5) the bending moment equals

$$M_U = P(x_C - x) + P \cot \psi_0 (y_C - y) = D \frac{d\psi}{ds} \quad (B-1)$$

where ψ is the angle between the slope and the horizontal, and s is the arc length from A to U measured along the elastic shape. Differentiating with respect to s , we get

$$D \frac{d^2\psi}{ds^2} = -P \frac{dx}{ds} - P \cot \psi_0 \frac{dy}{ds} = -P \cos \psi - P \cot \psi_0 \sin \psi \quad (B-2)$$

In terms of new variables

$$u = \frac{s}{L_2} ; \quad \theta = \psi + \psi_0 \quad (B-3)$$

the Equation 2 reduces to

$$\frac{d^2\theta}{du^2} + C^* \sin \theta = 0 \quad (B-4)$$

where $C^* = L_2^2 k_2^2$ and $k_2^2 = \frac{P}{D \sin \psi_0}$.

Further Equation 4 can be written in the form

$$\frac{1}{2} \left(\frac{d\psi}{du} \right)^2 = C^* \cos \theta + C_1 \quad (B-5)$$

For the solution of the constant C_1 we have the boundary condition

$$\left[\frac{d\psi}{ds} \right]_{\psi=\psi_2} = 0 \quad (B-6)$$

Therefore $C_1 = 0$, and

$$\frac{d\theta}{dU} = \sqrt{2C^* \cos \theta} \quad (B-7)$$

This equation can be integrated to give

$$\int_{L_1}^L ds = \frac{1}{2\sqrt{C^*}} \int_{\psi_1 + \psi_0}^{\pi/2} \frac{d\theta}{\sqrt{\sin^2 \pi/4 - \sin^2 \theta/2}} \quad (B-8)$$

To bring this Equation 8 to Legendre's standard form, let

$$P = \sin \pi/4; \quad p \sin \phi = \sin \theta/2 \quad (B-9)$$

In terms of the new variable ϕ , the Equation 8 reduces to

$$L_2 = \frac{1}{k_2} \left\{ \int_0^{\pi/2} \frac{d\phi}{[1-p^2 \sin^2 \phi]^{1/2}} - \int_0^m \frac{d\phi}{[1-p^2 \sin^2 \phi]^{1/2}} + \frac{1}{k_2} [K(p) - K(p, \bar{m})] \right\} \quad (B-10)$$

$$\text{where } \bar{m} = \sin^{-1} \left(\frac{1}{p} \sin \frac{\psi_1 + \psi_0}{2} \right)$$

The equation for the length s to the point u is given by

$$s_U = L_1 + \frac{1}{k_2} [K(p, n) - K(p, \bar{m})] \quad (B-11)$$

$$\text{where } n = \sin^{-1} \left(\frac{1}{p} \cdot \sin \left[\frac{\psi + \psi_0}{2} \right] \right) \quad (B-12)$$

The equation for the horizontal distance x to the point U is given by

$$\int_{x_B}^{x_U} dx = \int_m^n ds \cos \psi \quad (B-13)$$

Integrating this equation, we get

$$x_U = x_B + \frac{1}{k_2} \{ \cos \psi_0 [K(p, \bar{m}) - K(p, n) + 2E(p, n) - 2E(p, \bar{m})] + 2p \sin \psi_0 (\cos \bar{m} - \cos n) \} \quad (B-14)$$

The horizontal distance to the end of the cantilever C can be found by substituting $\psi = \psi_2$ and $n = \pi/2$ in Equation 14.

$$x_C = x_B + \frac{1}{k_2} (\cos \psi_0 [K(p, \bar{m}) - K(p) + 2E(p) - 2E(p, \bar{m})] + 2p \sin \psi_0 \cos \bar{m}) \quad (B-15)$$

The equation for the vertical distance y to the point U is given by

$$\int_{y_B}^{y_U} dy = \int_m^n ds \sin \psi \quad (B-16)$$

Integrating this equation,

$$y_U = y_B + \frac{1}{k_2} \{2p \cos \psi_0 (\cos \bar{m} - \cos n) - \sin \psi_0 [K(p, \bar{m}) - K(p, n) + 2E(p, n) - 2E(p, \bar{m})]\} \quad (B-17)$$

The vertical distance to the end of cantilever C is

$$y_C = y_B + \frac{1}{k_2} \{2p \cos \psi_0 \cos \bar{m} - \sin \psi_0 [K(p, \bar{m}) - K(p) + 2E(p) - 2E(p, \bar{m})]\} \quad (B-18)$$

For a point Q between A and B, Figure 3, the bending moment equals

$$M_Q = P(x_C - x) + P \cot \psi_0 (y_C - y) - P(x_B - x) - P \cot \lambda_0 (y_B - y) = D \frac{d\psi}{ds} \quad (B-19)$$

Differentiating with respect to s, we get

$$D \frac{d^2 \psi}{ds^2} = -P \cot \psi_0 \frac{dy}{ds} + P \cot \lambda_0 \frac{dy}{ds} = -k_1^2 \sin \psi \quad (B-20)$$

where $k_1^2 = (\cot \psi_0 - \cot \lambda_0) \frac{P}{D}$.

Equation 20 can be written as

$$\frac{1}{2} \left(\frac{d\psi}{ds} \right)^2 = k_1^2 \cos \psi + C_2 \quad (B-21)$$

For the solution of the constant C_2 we have the boundary condition

$$\left[\frac{d\psi}{ds} \right]_{\psi=\psi_1} = \sqrt{2} k_2 \sqrt{\cos(\psi_1 + \psi_0)}$$

Solving for C_2

$$C_2 = 2[k_2^2 \cos(\psi_1 + \psi_0) - k_1^2 \cos \psi_1] \quad (B-22)$$

Now the Equation 21 becomes

$$\frac{d\psi}{ds} = \sqrt{2} k_1 \sqrt{\left\{ (\cos \psi - \cos \psi_1) + \frac{k_2^2}{k_1^2} \cos(\psi_1 + \psi_0) \right\}} \quad (B-22)$$

Introducing a new variable p_1 such that

$$\frac{k_2^2}{k_1^2} \{\cos(\psi_1 + \psi_0)\} = 2p_1^2 - 1 + \cos \psi_1 \quad (B-23)$$

we can integrate the equation

$$\int_0^{L_1} ds = \frac{1}{2k_1} \int_0^{\psi_1} \frac{d\psi}{\sqrt{p_1^2 - \sin^2 \frac{\psi}{2}}} \quad (B-24)$$

To bring this Equation 24 to Legendre's standard form, let

$$\sin \psi / 2 = p_1 \sin \theta \quad (B-25)$$

Then

$$L_1 = \frac{1}{k_1} \int_0^N \frac{d\theta}{\sqrt{1-p_1^2 \sin^2 \theta}} = \frac{1}{k_1} k(p_1, N) \quad (B-26)$$

where $N = \sin^{-1} \left[\frac{1}{p_1} \sin \frac{\psi_1}{2} \right]$

The horizontal distance x to a point Q is given by

$$\int_0^{x_Q} dx = \int_0^{N_u} ds \cos \psi \quad (B-27)$$

$$x_Q = 3 \int_0^{N_u} \frac{d\theta}{\sqrt{1-p_1^2 \sin^2 \theta}} - 2 \int_0^{N_u} \sqrt{1-p_1^2 \sin^2 \theta} d\theta = \frac{1}{k_1} \{3[k(p_1, N_u) - 2E(p_1, N_u)]\} \quad (B-28)$$

where $N_u = \sin^{-1} \left[\frac{1}{p_1} \sin \frac{\psi}{2} \right]$

The horizontal distance x_B to the point Q is given by

$$x_B = \frac{1}{k_1} \left\{ 3[k(p_1, N) - 2E(p_1, N)] \right\} \quad (B-29)$$

where $N = \sin^{-1} \left[\frac{1}{p_1} \sin \frac{\psi_1}{2} \right]$

The vertical distance y to a point Q is given by

$$y = \int_0^y dy = \int ds \sin \psi = \frac{2p_1}{k_1} [1 - N_u] \quad (B-30)$$

The vertical distance y_B to the point B is given by

$$y_B = \frac{2p_1}{k_1} [1 - N] \quad (B-31)$$

REFERENCES

1. Piekutowski, A. J., "A Device to Determine the Out-of-Plane Displacements of a Surface Using a Moire Technique," AFWAL-TR-81-3005, March 1981.
2. Piekutowski, A. J., "Measurement of Out-of-Plane Displacements (User's Manual for the Moire Fringe Deflection Measurement Device)," AFWAL-TR-81-3006, March 1981.
3. Reinsch, C. H., "Smoothing by Spline Functions," Numerische Mathematik 10, 1967, pp. 177-183.
4. Rowlands, R. E., Liber, T., Daniel, I. M., and Rose, P. G., "Higher-order Numerical Differentiation of Experimental Information," Experimental Mechanics, Vol. 13, No. 3, 1973, pp. 105-112.
5. Berghaus, D. G. and Cannon, J. P., "Obtaining Derivatives from Experimental Data Using Smoothed-spline Functions," Experimental Mechanics, Vol. 13, No. 1, 1973, pp. 38-42.
6. Rowlands, R. E., Jensen, J. A. and Winters, K. D., "Differentiation Along Arbitrary Orientations," Experimental Mechanics, Vol. 18, No. 3, 1978, pp. 81-86.
7. Rowlands, R. E., Winters, K. D. and Jensen, J. A., "Full-field Numerical Differentiation," Journal of Strain Analysis, Vol. 13, No. 3, 1978, pp. 177-183.
8. MacBain, J. C., "Displacement and Strain of Vibrating Structures Using Time-average Holography," Experimental Mechanics, October 1978, pp. 361-372.
9. Bossaert, W., Dechaene, R. and Vinckiev, A., "Computation of Finite Strains from Moiré Displacement Patterns," Journal of Strain Analysis, Vol. 3, No. 1, 1968, pp. 65-75.

10. Frisch-Fay, R., Flexible Bars. Butterworths, 1962.
11. Frisch-Fay, R., "Large Deflections of a Cantilever Under Two Concentrated Loads," Journal of Applied Mechanics, March 1962, pp. 200-201.
12. Timoshenko, S. and Woinowsky-Krieger, S., Theory of Plates and Shells. McGraw-Hill Book Company, Inc., 1959, pp. 82-84.
13. Ashwell, D. G., "The Anticlastic Curvature of Rectangular Beams and Plates," Journal of Royal Aeronautical Society, Vol. 54, 1950, pp. 708-715.
14. Fung, Y. C. and Wittrik, W. H., "The Anticlastic Curvature of a Strip with Lateral Thickness Variation," Journal of Applied Mechanics, A.S.M.E. Vol. 76, Dec. 1954, pp. 351-358.
15. Fung, Y. C. and Wittrik, W. H., "A Boundary Layer Phenomenon in the Large Deflection of Thin Plates," Quart. Journal of Mechanics and Applied Mathematics, Vol. VIII, Pt. 2, 1955, pp. 191-210.

DAI
FILM